IMPROVEMENT OF MICROPHYSICAL PARAMETERIZATIONS THROUGH OBSERVATIONAL VERIFICATION EXPERIMENTS (IMPROVE)

Mark T. Stoelinga[a], Peter V. Hobbs[a], Clifford F. Mass[a], John D. Locatelli[a], Brian A. Colle[b], Robert A. Houze, Jr. [a], Arthur L. Rangno[a], Nicholas A. Bond[a, c], Bradley F. Smull[a, d], Roy M. Rasmussen [e], Gregory Thompson [e], and Bradley R. Colman [f]

Submitted for Publication to the *Bulletin of the American Meteorological Society*: 2 Jan. 2003

---

[a] Department of Atmospheric Sciences, University of Washington, Seattle, Washington

[b] Institute for Terrestrial and Planetary Atmospheres, State University of New York at Stony Brook, Stony Brook, New York

[c] Joint Institute for the Study of the Atmosphere and Ocean, University of Washington, Seattle, Washington

[d] NOAA/National Severe Storms Laboratory, Norman, Oklahoma

[e] Research Applications Program, National Center for Atmospheric Research, Boulder, Colorado

[f] National Weather Service, Seattle, Washington

Corresponding Author: Prof. Peter V. Hobbs
Department of Atmospheric Sciences, University of Washington
Box 351640, Seattle, WA 98195-1640
E-mail: phobbs@atmos.washington.edu

ABSTRACT

Despite continual increases in numerical model resolution and significant improvements in the forecasting of many meteorological parameters, progress in quantitative precipitation forecasting (QPF) has been slow. This is attributable in part to deficiencies in the bulk microphysical parameterization (BMP) schemes used in mesoscale models to simulate cloud and precipitation processes. These deficiencies have become more apparent as model resolution has increased. To address these problems requires comprehensive data sets that can be used to isolate errors in QPF due to BMP schemes from those due to other sources. These same data sets can then be used to evaluate and improve the microphysical processes and hydrometeor fields simulated by BMP schemes. In response to the need for such data, a group of researchers are collaborating on a study entitled IMPROVE (for Improvement of Microphysical Parameterizations through Observational Verification Experiments). IMPROVE has included two field campaigns carried out in the Pacific Northwest: an offshore frontal precipitation study off the Washington coast in January/February 2001, and an orographic precipitation study in the Oregon Cascade Mountains in November/December 2001. Twenty-six intensive observation periods yielded a uniquely comprehensive data set that includes in situ airborne observations of cloud and precipitation microphysical parameters; remotely sensed reflectivity, dual-Doppler, and polarimetric quantities; upper-air wind, temperature, and humidity data; and a wide variety of surface-based meteorological, precipitation, and microphysical data. These data are being used to test mesoscale model simulations of the observed storm systems, and in particular, to evaluate and improve BMP schemes used in such models. These studies should lead to improved QPF in operational forecast models.

Improvements in the representation of cloud and precipitation processes in mesoscale models are sought through comparisons of detailed field measurements with model outputs.

Regional mesoscale models are becoming increasingly important for short-term (0-48 h) operational forecasting of local weather systems and precipitation. However, despite significant improvements in the forecasting of many meteorological parameters, progress in quantitative precipitation forecasting (QPF) over the past several decades has been relatively modest (Olson et al. 1995; Fritsch et al. 1998). Furthermore, as model resolution has increased, problems with the cloud and precipitation fields have become increasingly apparent (Colle et al. 1999; Colle and Mass 1999; Colle et al. 2000). There are many aspects of an operational numerical weather prediction system that can contribute to errors in QPF: lack of sufficient initial data, deficiencies in data assimilation techniques, insufficient model resolution, numerical errors, and problems with parameterizations of boundary layer processes, convection, and bulk cloud and precipitation microphysics. In high-resolution models, bulk microphysical parameterization (BMP) schemes play a particularly important role in the model-produced QPF. However, comprehensive data sets needed to verify the physical processes and hydrometeor fields simulated by BMP schemes, and to isolate errors in BMP schemes from other sources of error, have not been available. To fill this need, we have embarked on a study entitled IMPROVE[1] (for Improvement of Microphysical Parameterizations through Observational Verification Experiments) to compare representations of cloud and precipitation processes in current mesoscale models with detailed observations in a variety of weather systems, with the goal of improving QPF produced by mesoscale models. In this paper we present the scientific background for IMPROVE, describe the design and operation of two IMPROVE field campaigns, present some examples of the data

[1] For more information on IMPROVE, visit the IMPROVE web site at http://improve.atmos.washington.edu.

obtained, and outline the direction of analysis and modeling research needed to achieve the goals of IMPROVE.

BACKGROUND. During the past three decades, the grid resolution of forecast models has increased with advances in computer technology, and model parameterizations of physical processes have become more sophisticated. Operational mesoscale models are only now approaching the resolution necessary to resolve the dynamical processes and key terrain features that have a direct and significant impact on precipitation. Several recent studies (Bruintjes et al. 1994; Colle and Mass 1996; Gaudet and Cotton 1998) have shown that, when run at sufficiently high resolution (down to ~10 km), mesoscale models can reproduce many of the observed features of precipitation structures over complex terrain. Yet, even when small-scale dynamical processes and complex terrain are adequately resolved, significant systematic deficiencies in model precipitation are often present (Colle et al. 1999; Colle and Mass 1999; Colle et al. 2000; Westrick and Mass 2001; Mass et al. 2002). For example, Colle et al. (2000) examined model precipitation bias, defined as simulated precipitation divided by observed at all available stations, for mesoscale model forecasts over the Pacific Northwest during the 1997-1999 cool seasons (Fig. 1). This measure showed that skill increased as grid spacing was reduced from 36 to 12 km, but then decreased as grid spacing was further reduced to 4 km.

These studies indicate that increased resolution alone is insufficient to produce quantitatively realistic QPF fields. Another key aspect of mesoscale models that affects QPF is the parameterization of cloud and precipitation processes. Mesoscale models running at <10 km resolution now treat most of the precipitation processes at the grid scale and, therefore, increasingly rely on sophisticated BMP schemes (e.g., Cotton 1982; Lin et al. 1983; Rutledge and Hobbs 1983, 1984), which until recently were used primarily in cloud resolving models. Remarkably, BMP schemes are now being used as sub-grid-scale precipitation parameterizations in global climate models (Grabowski 2001; Khairoutdinov and Randall 2001). Thus, the success or failure of BMP impacts model simulations on all scales (cloud, mesoscale, and global).

In BMP schemes, the explicit prediction of the mixing ratios of a limited number of cloud and precipitation hydrometeor types is based on a complex array of empirically and theoretically derived sources, sinks, and exchange terms between those hydrometeor types. In spite of their sophistication, evidence of flaws in these schemes is readily apparent, particularly for higher resolution simulations (e.g., Manning and Davis 1997; Colle and Mass 1999). However, these flaws have been generally revealed with indirect verification of the BMP scheme, such as comparing forecast and observed precipitation or satellite cloud cover during case studies. Such comparisons reveal problems in the BMP scheme, but they do not identify the origin of those problems. To clearly determine the source of problems in a BMP scheme (and to correct them) it is necessary to compare microphysical processes and predicted hydrometeor distributions in model simulations with in situ and remotely sensed observations. In addition, it is critically important that the microphysical measurements be obtained concurrently with observations of wind, temperature and humidity, so that errors in the simulated microphysics can be isolated from errors in other predicted fields. For example, in evaluating the moist physics parameterizations over terrain, it is crucial to determine the mesoscale wind, temperature, and humidity fields to ensure that errors in these basic state fields, perhaps due to model numerics or data assimilation, are not the source of the observed discrepancies.

Previous field programs that have included the study of cloud and precipitation microphysics [e.g., the Cascade Project (Hobbs et al. 1971), CYCLES (Hobbs 1978), the Sierra Cooperative Pilot Project (Reynolds and Dennis 1986), COAST (Bond et al. 1997), CASP-II (Cober et al. 1995), WISP (Rasmussen et al. 1992), and MAP (Binder et al. 1996)] did not obtain sufficiently comprehensive data sets for the evaluation of mesoscale models, due to either a lack of the key observing platforms and instruments or a lack of priority in the use of such platforms. This fact has been recognized by both the Eighth and Ninth Prospectus Development Teams of the U.S. Weather Research Program, whose reports (Fritsch et al. 1998 and Droegemeier et al. 2000, respectively) have placed high priority on observational testing of the parameterizations of cloud and precipitation microphysics in numerical weather prediction models.

SOME IMPORTANT MICROPHYSICAL ISSUES. A number of outstanding issues regarding cloud microphysical processes have arisen out of observational and modeling/parameterization studies. These issues provided specific areas for consideration by the IMPROVE project. Some of the more important areas and related questions include:

i) *Autoconversion of cloud water to rain water*:

- How important is it to predict or specify variable CCN concentrations (Chen and Lamb 1994; Rasmussen et al. 2002)?
- What is the general impact of increasing sophistication in the representation of autoconversion in model simulations, from the simplest scheme (Kessler 1969) to more complex schemes (e.g., Manton and Cotton 1977; Khairoutdinov and Kogan 2000)?
- Can/should aging effects be incorporated into the autoconversion process (Straka and Rasmussen 1997)?
- Do entrainment effects (Baker and Latham 1979; Telford and Wagner 1981) significantly hasten cloud-to-rain conversion?

ii) *Ice initiation*:

- Several approaches to relating ice nucleus concentrations to temperature and/or humidity have been proposed (Fletcher 1962; Cooper 1986; Meyers et al. 1992). Which should be used?
- Can/should aging effects be incorporated into the ice initiation process (e.g., Hobbs and Rangno 1985)?
- How important is the prediction of number concentration of ice particles (as opposed to predicting just mass concentration)?
- Rutledge and Hobbs (1983) artificially inserted the effects of generating cells into an idealized numerical simulation of the seeder/feeder process. To what extent do current

models handle the affect of generating cells aloft on stratiform precipitation, and does the process require a separate parameterization?

- Should ice nucleus number concentrations be treated as a predictive variable to more appropriately account for the depletion of ice nuclei (Rasmussen et al. 2002)?

iii) *Ice enhancement*:

- Ice splinter reproduction due to riming (Hallett and Mossop 1974; Mossop 1985) is the only ice enhancements process (if any) that is currently included in BMP schemes. However, there is evidence that ice enhancement can occur much faster than the Hallett/Mossop laboratory studies suggest (Hobbs and Rangno 1985, 1990; Rangno and Hobbs 1991, 1994). How should ice enhancement be parameterized in numerical models?

iv) *Ice particle terminal velocities*:

- Both empirical (e.g., Locatelli and Hobbs 1974; Zikmunda and Vali 1972) and theoretical (e.g., Mitchell 1996; Khvorostyanov and Curry 2002) expressions exist for relating ice particle size and terminal velocity for various crystal habits, degree of riming, and degree of aggregation. The challenge in designing BMP schemes is to assign a single terminal velocity relationship to each bulk hydrometeor category.

v) *Assumed precipitation size distributions*:

- Various levels of sophistication have been used in BMP schemes:
  a) exponential, with constant slope parameter;
  b) exponential, with slope parameter diagnosed from mixing ratio;
  c) exponential, with number concentration predicted; and,
  d) gamma distribution with specified diameter exponent

  Which approach is most appropriate and/or necessary for each hydrometeor type?

vi) *Aggregation*:

- Aggregation can have a significant effect on snow particle density [and thus, terminal fall velocity, as discussed by Rasmussen et al. (1999)] and snow size distribution (e.g., Lawson

et al. 1998). Aggregation is also temperature dependent (Hobbs et al., 1974). How is aggregation best represented in BMP schemes?

By utilizing the extensive and unique data gathered during the IMPROVE field studies, we will address these and other questions in an effort to improve BMP schemes in mesoscale forecast models.

GOALS OF IMPROVE. To meet the need for comprehensive observational data sets for testing and improving BMP schemes in mesoscale models, researchers at the UW initiated IMPROVE, with the following goals:

1. To obtain comprehensive, quantitative measurements of cloud microphysical variables for a variety of precipitation events in which models provide a realistic simulation of the larger scale structures. Such events should also produce a wide range of cloud and precipitation hydrometeor types and interactions.
2. To obtain corresponding dynamic and thermodynamic measurements (3D wind, temperature, and humidity) within and around the observed precipitation systems to provide the meteorological context in which the microphysical processes and precipitation events occurred.
3. To analyze the observational data to ascertain the physical processes leading to the development of precipitation, and the mixing ratios and size distributions of the various cloud and precipitation species.
4. To perform simulations of the observed cases with mesoscale models [the Penn State University/National Center for Atmospheric Research (NCAR) Mesoscale Model, Version 5 (MM5), and eventually the Weather Research and Forecast Model (WRF)] that include a state-of-the-art BMP scheme [e.g., the Reisner et al. (1998) mixed-

phase scheme], making use of the available observations in conjunction with advanced data assimilation techniques to maximize the accuracy of the simulations.

5. To compare the model forecasts of cloud and precipitation with the observations, both in terms of essential physical processes and quantitative amounts.
6. To make cost-effective and generally applicable improvements in BMP schemes in mesoscale models.

FIELD STUDY DESIGN. The need for comprehensive measurements was addressed through two IMPROVE field studies carried out in 2001. These field studies focused on clouds and precipitation forced by fronts and orography in the Pacific Northwest (see Fig. 2 for locations of study areas). In the winter, the Pacific Northwest is an ideal location to study precipitation systems both offshore and over orography, with numerous cyclonic storm systems making landfall from November through February.

IMPROVE-1, the Washington Offshore Frontal Field Study, was carried out off the coast of Washington State from 4 January–14 February 2001. The advantage of studying frontal systems over an oceanic domain with weak sea-surface temperature gradients is that they are driven by large-scale dynamical processes, which are typically well simulated in mesoscale models. Furthermore, because the lower boundary is spatially uniform, the structures of precipitation features can often be verified by observations even when modest timing and position errors are present.

IMPROVE-2, the Oregon Cascades Orographic Field Study, was carried out in the Oregon Cascade Mountains from 26 November–22 December 2001. Orographic precipitation systems are good candidates for IMPROVE studies because much of the forcing is tied to the terrain, and the terrain is precisely known. Thus, in situations where essentially steady flow impinges on a topographic barrier and the upstream conditions are known, the dynamical response to that flow is highly deterministic, provided the forecast model can properly resolve the key terrain-forced dynamics (Colle and Mass 1996). In addition, terrain-forced flow

produces large gradients in cloud microphysical variables and processes, which provides a good test bed for evaluating the model microphysics.

OBSERVATIONAL FACILITIES AND STRATEGIES. The IMPROVE field studies were designed to provide a multi-scale suite of measurements to document the chains of events that lead to the formation of precipitation in a variety of weather situations. Since a goal of IMPROVE is to isolate model deficiencies associated with cloud microphysical processes from those associated with dynamics (e.g., terrain or synoptically forced vertical air motions), in situ and remotely sensed measurements of cloud and precipitation structures, together with simultaneous Doppler radar measurements of the kinematic field, were required. The 3-D wind field measurements provided by Doppler radar can be compared with model simulations to see if the model captures the essential dynamics. In addition, long-range ground based radar was essential for short-term weather forecasting, the guidance of research aircraft into precipitation systems, and the mapping of mesoscale precipitation structures and evolutions. The specific observing systems used to fill these needs, as well as other supporting observing systems, are listed in Table 1. The locations of all the observing systems during IMPROVE-1 and IMPROVE-2 are illustrated in Figs. 3 and 4, respectively, and are described in more detail below. The wide array of facilities described here provided an unprecedented set of measurements for documenting cloud and precipitation processes on scales ranging from the microphysical to the synoptic.

IMPROVE-1: The Washington Offshore Frontal Study. The primary facilities used during IMPROVE-1 were the UW Convair-580 research aircraft and NCAR's S-band polarimetric (S-Pol) Doppler radar [augmented with a bistatic network (BINET) of two antennas]. The range of the radar, as well as our interest in studying offshore systems, defined the boundary of the study area, shown by the heavy blue line in Fig. 3.

The UW's Convair-580 aircraft was well suited to obtain detailed in situ measurements of thermodynamic state parameters, cloud structure and precipitation properties. Also aboard were instruments for measuring aerosol properties, and a 35 GHz (cloud) radar. Instruments of particular importance were the SPEC Cloud and Precipitation Particle Imager (CPI), which provides quantitative information on the concentrations and size distributions of liquid and solid cloud and precipitation particles from 5 μm to 2.5 mm with a resolution of 2.3 μm (Lawson and Jensen 1998); the SPEC High Volume Precipitation Sampler (HVPS), which measures the size spectrum and precipitation particles from 200 μm to 5 cm with a resolution of 200 μm with ~1 m^3 s^{-1} sampling rate at an aircraft speed of 100 m s^{-1} (Lawson et al. 1993); three Particle Measuring Systems (PMS) probes (FSSP-100, 1D-C and 2D-C) for cloud particle identification and sizing; and several instruments for measuring liquid water content (LWC) of clouds. Figure 5 shows the size ranges of particles covered by these various instruments.

The NCAR S-Pol radar, which was located at Westport on the Washington Coast (Fig. 3), has a wavelength of 10 cm and dual-polarization capabilities. The dual-polarized radar measurements can be used to infer information on particle type (wet snow, dry snow, irregular ice, rain) (Doviak and Zrnic 1993; Vivekanandan et al. 1999). Through the use of two bistatic receiving antennas in conjunction with a single ground-based Doppler radar, 3-D air motions can be inferred using precipitation particles as targets (Wurman et al. 1993; Wurman 1994). For this purpose, bistatic receivers were located ~60 km north and south of the S-Pol radar. The bistatic antennas retrieved Doppler velocities from regions with reflectivities $\gtrsim$11 dBZ.

Additional facilities used in IMPROVE-1 included a number of rain gauges along the coast, National Weather Service (NWS) rawinsonde launches from Quillayute, Washington, and Salem, Oregon, every 3 h on request; rawinsonde launches from Westport on the central Washington coast (by the U.S. Navy) on request; a 915 MHz wind profiler and radio acoustic sounding system (RASS) for continuous vertical profiles of wind and temperatures in the lower atmosphere, operated by the Environmental Technology Laboratory (ETL) of the National Oceanic and Atmospheric Administration (NOAA); a scanning microwave radiometer deployed

by NCAR at the S-Pol site in Westport; and, the Pacific Northwest National Laboratory (PNNL) Atmospheric Remote Sensing Laboratory (PARSL), consisting of a 94-GHz vertically pointing cloud radar, a surface meteorology instrument suite, an optical rain gauge, a variety of radiometers for measurement of downwelling radiation, a total sky imager, a microwave radiometer, and a ceilometer, all of which were located at Pacific Beach, ~40 km north of Westport.

The primary strategic challenges in IMPROVE-1 were the flight-track design and targeting of the Convair-580 flight tracks for optimal microphysical data gathering; the optimal scan strategy for the S-Pol radar for weather surveillance, polarimetric studies, and dual-Doppler coverage; and the timing of special sonde launches. The Convair-580 flight tracks (see Figs. 6a and 6c) were designed to probe regions of banded precipitation along a stacked series of alternating horizontal and ascending flight legs oriented perpendicular to the band, at a variety of vertical levels. When possible, the aircraft flew along a radial from the radar so that its cross sectional plane could be viewed in a single range-height indicator (RHI) radar scan. The lowest leg was flown just below the melting level to ascertain the liquid precipitation rate. End points of the legs were radioed to the aircraft in real time by a scientist at the radar site who could plot the aircraft location on a real-time radar display of the rainband. The S-Pol radar scanning strategy consisted of a ~30-min repeating cycle that included low-elevation surveillance scans, dual-Doppler sector volumes, and RHI scans along selected azimuths. Sondes were launched at the NWS sites at Quillayute and Salem, as well as at Westport, at 3-hour intervals during a 9-12 hour period bracketing the aircraft flight(s) in order to capture the frontal structure associated with the precipitation bands in which the aircraft flew.

IMPROVE-2: The Oregon Cascades Orographic Study. In IMPROVE-2, the UW's Convair-580 research aircraft was again used to obtain in situ measurements and was joined by a NOAA P-3 aircraft. The instruments aboard the Convair-580 were essentially the same as in IMPROVE-1; exceptions were that the 35 GHz radar and the CPI were generally not operational,

and a cloud condensation nucleus (CCN) counter was installed and operated by NCAR personnel. Due to the complex terrain, an airborne dual-Doppler radar system was used during IMPROVE-2 instead of the ground-based binet system. The fore/aft-scanning Doppler X-band radar aboard the NOAA P-3 aircraft provided 3-D air motions, particularly in the regions that the Convair-580 acquired cloud microphysical measurements. The P-3 was also instrumented for basic state parameter measurements, and had aboard PMS cloud and precipitation probes and an instrument for measuring cloud LWC. The NCAR S-Pol radar was located on a hill top (473 m above sea level) near Sweet Home, Oregon. This location provided unblocked views to the west for surveillance of approaching weather, and to the east for describing the mesoscale and microphysical aspects of precipitation in the upslope zone.

Additional facilities used in IMPROVE-2 included three mobile observers to identify snow crystal types reaching the surface at various locations across Santiam Pass; special NWS rawinsonde launches from Salem, Oregon, at 3-h intervals on request; a UW mobile rawinsonde unit; two NOAA/ETL 915 MHz wind and temperature profile units, located at Newport on the Oregon Coast and at McKenzie Bridge, Oregon, immediately to the west of the Cascade Crest; the NCAR Integrated Sounding System (ISS), consisting of a 915 MHz Doppler clear-air wind profiling unit, a RASS for temperature profiles, and a surface observing station, at Halsey, Oregon, in the Willamette Valley, and at Black Butte Ranch, Oregon, on the lee of the Cascades; a sonde unit at the Black Butte ISS site; a NOAA/ETL vertically-pointing S-band Doppler radar, for providing information on precipitation structures aloft, located at McKenzie Bridge; five all-weather rain gauges along Highway 20 across Santiam Pass; a Radiometrics scanning microwave radiometer, operated by NCAR, for measuring time series of column-integrated LWC and water vapor (Hogg et al. 1983; Heggli et al. 1983) at Santiam Pass; the PARSL in situ and remote sensing observing suite (same as in IMPROVE-1) on the eastern side of the Cascade Crest at Sisters, Oregon; and, a disdrometer for drop size distribution measurements at McKenzie Bridge.

The primary strategic challenges in IMPROVE-2 were the targeting, flight-track design, and flight coordination of the Convair-580 and P-3 aircraft for optimal microphysical data gathering and dual-Doppler radar coverage; the optimal scan strategy for the S-Pol radar for weather surveillance and polarimetric studies; and the timing of special sonde launches. As in IMPROVE-1, the Convair-580 flight tracks in IMPROVE-2 (see Figs. 6b and 6d) were designed to probe precipitation features along a stacked series of horizontal flight legs, but in IMPROVE-2 the orientation of the stack was along one of two tracks, referred to as the W-E track and the SW-NE track. Both tracks passed directly over Santiam Pass. The choice of track was based on the desire to fly roughly parallel to the mean wind direction in the lower to middle troposphere. The lowest leg of the track was flown along a terrain-following minimum safe altitude, which was typically ~1.5 km above the underlying terrain. Endpoints for the flight legs were radioed to the Convair-580 by a scientist stationed at the S-Pol radar. The P-3 flew repeated "lawnmower" patterns of five north/south legs, each at a constant, minimum safe altitude, 139 km long and spaced 37 km apart, to map out the Doppler velocity structure over the same area that in situ measurements were obtained from the Convair-580. The S-Pol radar scanning strategy consisted of a ~12-min repeating cycle that included low-elevation 360º surveillance scans, and a sector of closely spaced RHIs aimed up the mountain slope. Sondes were launched from the NWS site at Salem, Oregon, from the mobile unit in the Willamette Valley, and from the ISS site at Black Butte, at ~3-h intervals during a 9-12 h period bracketing the aircraft flight(s) to capture the upstream and lee-side vertical profile of wind, temperature, and humidity.

A major operational challenge in IMPROVE-2 was the often severe aircraft icing experienced by both aircraft as they flew in supercooled orographic clouds. As illustrated by the ice cap on the nose of the NOAA P-3 after a research flight (Figure 7), thick ice accumulated on aircraft windshields and airframes, occasionally to such a degree that flight legs had to be either ended or paused while the aircraft descended to warmer regions. Icing resulted in several aircraft component failures, including the deicing boot on a P-3 prop and an airspeed indicator on the Convair-580. Ice breaking off and impacting on the fuselage of the aircraft often

produced disquieting banging, and on one occasion icing had a noticeably detrimental impact on the flight characteristics of the P-3.

FIELD STUDY OPERATIONS. During both field phases, aircraft and other manned operations were on standby for activation between 7 AM and 10 PM local time. This schedule lent itself to a regular daily routine, with a Daily Planning Meeting held every day at 1 PM, and three forecasting shifts that were assigned to a rotating crew of forecasters from the UW. At the Daily Planning Meeting, IMPROVE scientists and other interested persons gathered to discuss the weather forecast and possible field operations for the remainder of the current day and the next day, and to make a preliminary decision on whether or not to call an Intensive Observation Period (IOP) for the next day. Discussions also took place in the evening and early morning to refine operational plans based on current forecast model guidance, satellite observations, etc.

The conduct of each IOP involved coordinated efforts of many groups and individuals at widely scattered observational sites. Some of the activities, and the sites at which they occurred, are shown in Fig. 7.

INTENSIVE OBSERVING PERIODS. The winter of 2000/2001 (during which IMPROVE-1 was conducted) was drier than normal in the Pacific Northwest, whereas, the following winter (during which IMPROVE-2 was conducted) was wetter than normal. However, both field phases provided several opportune weather systems for studying the targeted types of clouds and precipitation. Figure 8 shows precipitation time series from two selected special raingauges, one from IMPROVE-1 and one from IMPROVE-2, with the time periods of IOPs overlaid.

Precipitation during IMPROVE-1 was below normal due to a persistent split flow pattern. For example, Hoquiam, on the central Washington Coast, received 16.7 and 10.8 cm during January and February, respectively, compared to climatological values of ~24.7 and 20.9 cm for these months. The precipitation at another Washington coastal location (Kalaloch) indicates that the IOPs generally coincided with periods of measured precipitation at the coast

(Fig. 8). The correspondence was not perfect due in part to the persistent upper-level split flow, which caused some systems that were studied offshore to never make landfall or to weaken considerably upon landfall, whereas, other systems made landfall after offshore observations were terminated. The majority of the IMPROVE-1 events were weak to moderate strength occlusions, which are climatologically the most frequent type of frontal passage in the area. Generally, model forecasting guidance was skillful and nearly all candidate weather systems were successfully targeted; a notable exception was a vigorous warm-frontal system on the evening of 3 February, which was missed due to poor model guidance.

The IMPROVE-2 period was considerably wetter than normal over central Oregon. Persistent zonal flow or troughing over the eastern Pacific brought a series of strong cyclones and fronts across the region during the first three weeks of the experiment. Stations in the Orographic Study Area generally received half a standard deviation above the normal precipitation amount for the month of December. For example, McKrenzie Bridge, on the western slopes of the Oregon Cascades, received 37.9 cm during December, 10.8 cm above normal, while the nearby special IMPROVE-2 raingauge at Falls Creek recorded a total of over 40.0 cm over the 4-week study period (Fig. 8b). Forecasting for IMPROVE-2 was challenging: some periods of heavy orographic precipitation were not well predicted by the models for forecast times over 24 h. However, the strongest and wettest weather systems were accurately targeted by IMPROVE operations.

A variety of flow regimes, frontal systems, and rainbands characterized both field phases of IMPROVE. The specific types of precipitation systems that were studied in all of the IOPs of both field phases are listed in Tables 2 and 3. To illustrate the types of data gathered, two cases, one from each field phase of IMPROVE, are discussed briefly below. Detailed studies of these and other IMPROVE cases, and comparisons with numerical model outputs and algorithms, will be described in a future issue of the *Journal of the Atmospheric Sciences.*

IMPROVE-1: 1 February 2001. In mid-afternoon on 1 February, a strong occluded cyclone developed in the northeast Pacific Ocean, with an ill-defined warm front straddling the coast and a cold/occluded front moving steadily shoreward (Fig. 9). A deep cloud band is evident ahead of the front. A time-height cross-section (Fig. 10), constructed from coastal soundings (at Quillayute and Westport—see Fig. 3), indicates that the frontal system was occluded as it came ashore, with a strong upper-level cold front forcing the main precipitation band, and a trailing surface occluded front making landfall several hours later. The warm-frontal surface can be seen as a stable layer (i.e., a layer of tightly packed contours of potential temperature and equivalent potential temperature) at ~800 hPa, ahead of the upper cold front. The rainband associated with the upper cold front was ~100 km wide, and was quite vigorous as it passed through the study area, with extensive, fairly uniform radar echoes of 35-40 dBZ over a wide area. The Convair-580 aircraft intercepted the rainband and flew a vertical stack of horizontal legs through it from 2347 UTC 01 Feb to 0253 UTC 02 Feb.

One issue that is of particular interest in IMPROVE is the role and importance of upper-level generating cells in the development of stratiform precipitation. Previous research has shown that contributions to precipitation mass by generating cells range from ~20% (Hobbs et al., 1980) to ~35% (Houze et al., 1981) depending on the strength of vertical air motions in the "feeder" zone. However, these cells tend to be small in scale and convective in nature, and it is not clear how well mesoscale models simulate stratiform precipitation that is influenced by generating cells aloft, and whether this phenomenon requires a separate parameterization scheme. Analysis of the S-Pol radar data shows that the 1 February rainband was rife with generating cells at two altitudes. These can be seen most clearly in RHI scans from the S-Pol radar through the leading edge of the band (Fig. 11). A cirrus layer of generating cells is seen around 10 km altitude, and an altocumulus layer of generating cells at around 6 km altitude. Fallstreaks can be seen emanating from the generating cells, particularly from those in the altocumulus layer. In the later RHI scan (Fig. 11b), the fallstreaks penetrate the melting layer bright band (at ~1-2 km) and appear to enhance the precipitation reaching the ground.

Figure 12 shows a cross section through the rainband from the S-Pol radar along the same vertical section flown by the Convair-580. The color code shows the polarimetrically-derived particle type identification (Vivekanandan et al. 1999). The precipitation regime is fairly uniform over a wide horizontal region, with the melting band (as seen in the transition from dry snow to wet snow to rain) occurring at around 1.5 km. The system-relative aircraft flight track is also shown, and the clutter signal from the aircraft can be seen as a narrow magenta colored area at the nose of the overlaid aircraft symbol.

During the course of the 2 h and 20 min period that the Convair-580 flew in the rainband in temperatures below freezing, over 90,000 images of ice crystals were generated by the CPI. Each image was examined to determine crystal type and degree of riming. This detailed information is being studied to determine the precipitation processes involving the generating cells. Figure 12 shows representative examples of some of the crystal types encountered during the flight.

On the highest leg of the flight through the rainband, unrimed bullets (both radiating assemblages as seen in Fig. 12a and single bullets) were seen; these crystals likely originated in the cirrus generating cells. Beneath that level, radiating assemblages of sideplanes (Fig. 12b) and assemblages of plates (Fig. 12c) were found, which probably originated in the altocumulus generating cells. Lower still were columns and bullets with plates on their ends (Fig. 12d, e), which originated at higher levels. At the lowest levels, sheaths (Fig. 12f), as well as plate-like crystals that originated aloft but subsequently grew sheaths and columns normal to their faces (Fig. 12g), were encountered. This type of information on crystal types, in conjunction with particle mass concentrations and size distributions, can be used to derive the growth history and spatial distribution of precipitation, which can be compared with model-simulated processes for the formation of the precipitation.

IMPROVE-2: 13 December 2001. On the afternoon of 13 December 2001 a vigorous frontal system, associated with a deep low-pressure center that tracked into Vancouver Island, came

onshore in Oregon (Fig. 13). Although there did not appear to be a classical warm or occluded front with this system, the cold front had a tipped-forward structure in the lowest 3 km, not unlike the case discussed above from the IMPROVE-1 field study. The strongest synoptically forced precipitation occurred ahead of the upper cold front in a band that brought widespread stratiform precipitation to the study area for several hours. In addition to the synoptically forced precipitation, strong low-level flow with a large cross-barrier (westerly) component resulted in significant orographic enhancement of precipitation on the windward slopes of the Cascades. This situation is distinctly different from that typically seen in the Washington Cascades during the CASCADE Project (Hobbs et al. 1971), in which strong low-level cross barrier flow and orographic precipitation development was typically not present until after frontal passage. Thus, in the 13 December 2001 case, the prefrontal regime had a combination of strong synoptically forced precipitation production aloft and strong orographic forcing below, resulting in heavy precipitation on the windward slopes of the Cascades. All of the IMPROVE-2 observational assets were deployed during this precipitation event. The Convair-580 aircraft performed two vertical stacks for in situ microphysical measurements, one in the prefrontal regime and one in the postfrontal regime, and the P-3 aircraft carried out nearly two complete lawn-mower patterns for dual-Doppler measurements.

The combination of forcing mechanisms discussed above is evident in several aspects of the measurements. A time series from the microwave radiometer that was situated 7 km west of the Cascade crest (Fig. 14) illustrates the temporal evolution of column-integrated LWC. The time series indicates that the highest values of liquid water (and by inference, the strongest orographic forcing) occurred not in the postfrontal regime, but simultaneously with the rainband that was immediately ahead of the upper-level front. A cross section in the vertical plane in which the Convair-580 completed its first vertical stack is shown in Fig. 15. This flight was almost entirely within the rainband ahead of the upper-level front. Along the flight track are shown several representative images from the PMS 2D-C probe. The schematically drawn fallstreaks indicate the region where ice particles generated by the rainband either fell into the

flight region from above or developed within the flight region. The schematically drawn cloud boundary indicates the top of a region where the aircraft encountered significant supercooled liquid water. Examples of liquid water droplet images are seen just below the 4 km level. Beneath that level, both high supercooled liquid water and high ice particle concentrations (e.g., needles and aggregates thereof at around 3 km) coexisted, indicating the vigor of the liquid water-replenishing orographic uplift. Some evidence of rimed aggregates (i.e., aggregates with few interstitial spaces) are seen just above the freezing level. Also, a polarimetrically derived particle identification plot from an RHI scan of the S-Pol radar in the upslope direction (Fig. 16) indicated the existence of graupel (green and dark green colors) just above the melting band.

A high-resolution time series of reflectivity (Fig. 17a) from the S-band vertical profiler at McKenzie Bridge (approximately 20 km west of the Cascade crest) indicates a deep continuous layer of echo with a bright band at a height of 1.7 km prior to 0200 UTC 2 Feb. The radial velocity data (Fig. 17b) showed a considerable depth between 2.0 and 3.5 km in which the radial velocity was zero or upward, indicating updraft of a meter per second or more. The image shows a pattern of closely spaced convective-scale cells of upward air velocity, just above the melting layer. This pattern is consistent with the appearance of graupel at this level in the S-Pol particle identification field, providing another indication of both the large input of ice particles from aloft and the strong production of supercooled liquid water by orographic uplift.

SOME PRELIMINARY MODELING STUDIES. Model simulations of both the 1 February 2001 and 13 December 2001 cases described above have been run at 4-km horizontal resolution, with coarse-grid simulations (36 and 12-km resolution) supplying the boundary conditions. Preliminary work has been completed to verify that the simulations captured the essential kinematic, thermal, and moisture structures that were observed. Vertical cross sections of the two model simulations are shown in Fig.18. The model cross sections are in the same vertical plane as the Convair-580 flight tracks along which cloud microphysical data were collected. In both model simulations, the equivalent potential temperature (θ_e) pattern shows an occluded

baroclinic structure entering the picture from west to east (left to right), with an axis of maximum θ_e sloping eastward with height in the lowest 4 km. Although the two cases share this basic synoptic structure, they differ in terms of the presence of orographic forcing in the IMPROVE-2 case, and in terms of greater static stability in the IMPROVE-1 case (note that in Fig. 18a, the θ_e contours are more closely spaced in the vertical and the temperature contours more widely spaced, both of which indicate greater stability). Both model simulations produce regions of cloud water, rain, cloud ice, snow, and graupel, with significant amounts of supercooled liquid water.

Precipitation amounts predicted by the MM5 model at 4-km grid spacing for 13-14 December 2001 were checked using over 100 hourly cooperative observer (COOP) and snow telemetry (SNOTEL) sites across Oregon and southern Washington (Fig. 19). The MM5 precipitation accumulated between 1400 UTC 13 December and 0800 UTC 14 December was interpolated to the observation sites using a Cressman (1959) weighting method (Colle et al. 1999). Figure 19 shows the percentage of the observed precipitation produced by the model at the observation sites. The model over-predicted the precipitation over the Cascades, while there is some under-prediction in the lee of the coastal range. The over-prediction occurred even though the model-simulated crest-level flow was 5-10 m s^{-1} weaker than observed (not shown), which suggests deficiencies in the model microphysics.

CURRENT AND FUTURE RESEARCH DIRECTIONS. IMPROVE research is now focusing on two main efforts: analysis of the observational data and model simulations. Both the observational and modeling studies can be divided into three main objectives: (1) to understand and quantify the mesoscale processes that lead to the development and modulation of precipitation; (2) to understand and quantify the microphysical processes that lead to the development of precipitation; and, (3) to quantify the spatial and temporal distributions of cloud and precipitation hydrometeors and precipitation fallout at the surface. For each of these objectives, the goal is the comparison of model outputs with the observations. The mesoscale

kinematic, thermal, and moisture evolution in the model simulation will be checked and errors reduced to a minimum; any remaining errors in the precipitation evolution can be attributed to the BMP scheme used in the model simulation. For example, specific phenomena that will be examined are the model's handling of mountain waves in the orographic cases (Reinking et al. 2000) and of upper-level instability and generating cells in deep frontally forced precipitation systems (Hobbs et al. 1980; Houze et al. 1981). Incorrect kinematic fields associated with these phenomena will likely affect the accuracy of the model-simulated precipitation, irrespective of possible problems in the BMP scheme. We will attempt to correct these kinematic and dynamical deficiencies using tools such as 4D data assimilation on the outer grids. The microphysical processes and quantitative outputs from the model will be compared with observations to determine where the BMP scheme is handling precipitation development properly and where it is not. These comparisons should reveal any weaknesses in the BMP schemes and motivate improvements. The revised schemes will then be tested on other IMPROVE cases and in an operational forecasting environment.

COOPERATIVE EFFORTS. In addition to the primary goals of IMPROVE, several participants were able to incorporate other research and operational efforts into the field studies, which took advantage of the substantial observational assets provided by IMPROVE:

- During IMPROVE-1, the NWS was keenly interested in operational use of the S-Pol radar that was deployed on the Washington coast, since it was placed in a location that fills in a major gap in coverage of the operational WSR-88D radar network, and it has polarimetric capabilities. NCAR set up a Zebra display workstation in the NWS-Seattle office, providing NWS with real-time access to S-Pol reflectivity, Doppler velocity, particle identification, and rainfall estimation plots. These products were examined routinely by forecasters and were helpful in predicting some heavy precipitation events on the Olympic Peninsula. The NWS in turn contributed to IMPROVE with forecasting

assistance and with special sonde launches at Quillayute, Washington, and Salem, Oregon, during both field phases of IMPROVE.

- The PNNL deployed their PARSL remote sensing observing system to test its suite of cloud sensing measurements against in situ microphysical measurements from the aircraft. They also contributed surface and radar observations to the IMPROVE data set, and provided a sounding receiver unit during IMPROVE-2.
- In conjunction with the PACJET field program, which occurred along the west coast of the U.S. simultaneously with IMPROVE-1, NOAA/ETL deployed a 915-MHz wind profiler site at Westport, approximately 1 km from the S-Pol radar site. This site benefited both PACJET and IMPROVE, and provided an opportunity to perform intercomparison between the wind profiles provided by a 915-MHz wind profiler and by velocity-azimuth display (VAD) scans from a 10-cm radar (such as S-Pol or WSR-88Ds).
- During IMPROVE-2, NCAR's Research Applications Program (RAP) installed a CCN counter on the Convair-580 and, on some missions, CCN concentrations were measured in the westerly flow upstream of the Cascade Range prior to cloud formation, and in cloud-processed air in the lee of the Cascades.
- NCAR/RAP also participated in Convair-580 research flights during IMPROVE-2 to study the development of supercooled liquid water and in-flight icing conditions. Such conditions occurred on several flights during IMPROVE-2, particularly during postfrontal orographic precipitation events.
- Sandra Yuter (UW) deployed two disdrometers at McKenzie Bridge, collocated with the NOAA/ETL profilers and surface meteorology instruments, to add another precipitation site to her data set on raindrop size distributions in diverse locations.

SUMMARY. During the past several years, there has been increasing evidence for deficiencies in bulk microphysical parameterizations in numerical weather prediction models. Improvements in these parameterizations have been difficult because coincident and comprehensive

measurements of both the basic state flow and microphysical parameters have not been available. In response to the need for such data, two field campaigns were carried out: an offshore frontal precipitation study off the Washington coast in January/February 2001, and an orographic precipitation study in the Oregon Cascade Mountains in November/December 2001. Twenty-six intensive observation periods yielded a uniquely comprehensive data set that includes in situ airborne observations of cloud and precipitation microphysical parameters; remotely sensed reflectivity, dual-Doppler, and polarimetric quantities from both the surface and aloft; upper-air wind, temperature, and humidity data from both balloon soundings and vertical profilers; and a wide variety of surface-based meteorological, precipitation, and microphysical data. These data are being used to test mesoscale model simulations of the observed storm systems and, in particular, to evaluate and improve bulk microphysical parameterization schemes used in the models. These studies should lead to improved quantitative precipitation forecasting in research and operational forecast models.

A comprehensive description of IMPROVE and its data sets are available on the IMPROVE web site: http://improve.atmos.washington.edu.

Acknowledgments. Thanks are due to NCAR (Atmospheric Technology Division and Research Applications Program), NOAA/ETL, and PNNL for providing and staffing experimental facilities; the NWS and the Naval Pacific Meteorology and Oceanography Facility at Whidbey Island, for launching special rawinsondes on request; the NOAA P-3 team; the Convair-580 pilots; and the Federal Aviation Administration/Seattle Air Route Traffic Control Center for cooperation in the use of airspace.

IMPROVE is funded by the Mesoscale Dynamic Meteorology Program (Stephan Nelson, Program Director) and the Physical Meteorology Program (Roddy R. Rogers, Program Director) of the Division of Atmospheric Sciences, National Science Foundation (NSF), and by the U.S. Weather Research Program. NCAR's participation in IMPROVE was sponsored by the National Science Foundation and the Federal Aviation Administration.

REFERENCES

Baker, M.B., and J. Latham, 1979: The evolution of droplet spectra and the rate of production of embryonic raindrops in small cumulus clouds. *J. Atmos. Sci*., **36**, 1612–1614.

Binder, P., and co-authors, 1996: MAP—Mesoscale Alpine Programme design proposal. MAP Programme Office, 77 pp. [Available from MAP Programme Office c/o Swiss Meteorological Institute, Krähbühlstrasse 58, CH-8044 Zürich, Switzerland.]

Bond, N. A., and co-authors, 1997: The Coastal Observation and Simulation with Topography (COAST) experiment. *Bull. Amer. Meteor. Soc*., **78**, 1941-1955.

Bruintjes, R. T., T. L. Clark, and W. D. Hall, 1994: Interactions between topographic airflow and cloud/precipitation development during the passage of a winter storm in Arizona. *J. Atmos. Sci.*, **51**, 48-67.

Chen, J.-P., and D. Lamb, 1994: Simulation of cloud microphysical and chemical processes using a multicomponent framework. Part I: Description of the microphysical model. *J. Atmos. Sci*., **51**, 2613–2630.

Cober, S. G., G. A. Isaac, and J. W. Strapp, 1995: Aircraft icing measurements in east coast winter storms. *J. Appl. Meteor*., **34**, 88–100.

Colle, B. A., and C. F. Mass, 1996: An observational and modeling study of the interaction of low-level southwesterly flow with the Olympic Mountains during COAST IOP 4. *Mon. Wea. Rev*., **124**, 2152–2175.

_____, and _____, 1999: The 5-9 February 1996 flooding event over the Pacific Northwest: Sensitivity studies and evaluation of the MM5 precipitation forecasts. *Mon. Wea. Rev*, **128**, 593-617.

_____, K. Westrick, and C. F. Mass, 1999: Evaluation of MM5 and Eta-10 precipitation forecasts over the Pacific Northwest during the cool season. *Wea. Forecasting*, **14**, 137-154.

_____, C. F. Mass, and K. J. Westrick, 2000: MM5 precipitation verification over the Pacific Northwest during the 1997–99 cool seasons. *Wea. Forecasting*, **15**, 730–744.

Cooper, W. A., 1986: Ice initiation in natural clouds. *Precipitation Enhancement—A Scientific Challenge, Meteor. Monogr.,* No. 21, Amer. Meteor. Soc., 29–32.

Cotton, W. R., 1982: Colorado State University three-dimensional cloud/mesoscale model. Part 2: Ice phase parameterization. *J. Rech. Atmos*., **16**, 295-320.

Cressman, G., 1959: An operational objective analysis system. *Mon. Wea. Rev*., **87**, 367-374.

Doviak, R. J., and D. S. Zrnic, 1993: *Doppler Radar and Weather Observations*. 2d ed. Academic Press, 562 pp.

Droegemeier, K. K., and co-authors, 2000: Hydrological aspects of weather prediction and flood warnings: Report of the Ninth Prospectus Development Team of the U.S. Weather Research Program. *Bull. Amer. Meteor. Soc.*, **81**, 2665–2680.

Fletcher, N. H., 1962: *Physics of Rain Clouds.* Cambridge University Press, 386 pp.

Fritsch, J. M., and co-authors, 1998: Quantitative precipitation forecasting: report of the eighth prospectus development team, U. S. Weather Research Program. *Bull. Amer. Meteor. Soc.*, **79**, 285-299.

Gaudet, B., and W. R. Cotton, 1998: Statistical characteristics of a real-time precipitation forecasting model. *Wea. Forecasting*, **13**, 966–982.

Grabowski, W. W., 2001: Coupling cloud processes with the large-scale dynamics using the cloud-resolving convection parameterization (CRCP). *J. Atmos. Sci.*, **58**, 978-997.

Hallett, J., and S. C. Mossop, 1974: Production of secondary ice crystals during the riming process. *Nature,* **249,** 25–28.

Heggli, M. F., L. Vardiman, R. E. Stewart, and A. Huggins, 1983: Supercooled liquid water and ice crystal distributions within Sierra Nevada winter storms**.** *J. Appl. Meteor.*, **22**, 1875–1886.

Hobbs, P. V., 1978: Organization and structure of clouds and precipitation on the mesoscale and microscale in cyclonic storms. *Rev. Geoph. and Space Phys.*, **16**, 741-755.

_____, and A. L. Rangno, 1985: Ice particle concentrations in clouds. *J. Atmos. Sci.,* **42,** 2523-2549.

_____, and A. L. Rangno, 1990: Rapid development of high ice particle concentrations in small polar maritime cumuliform clouds. *J. Atmos. Sci.,* **47,** 2710–2722.

_____, L. F. Radke, A. B. Frasier, and R. R. Weiss, 1971: The Cascade Project: A study of winter cyclonic storms in the Pacific Northwest. *Proc. Intl. Conf. Wea. Modif.*, Canberra, Australia.

_____, S. Chang, and J. D. Locatelli, 1974: The dimensions and aggregation of ice crystals in natural clouds. *J. Geophys. Res.,* **79,** 2199-2206.

_____, T. J. Matejka, P. H. Herzegh, J. D. Locatelli, and R. A. Houze Jr., 1980: The mesoscale and microscale structure and organization of clouds and precipitation in midlatitude cyclones. I: A case study of a cold front. *J. Atmos. Sci.*, **37**, 568–596.

Hogg, D.C., F.O. Guiraud, J.B. Snider, M.T. Decker, and E.R. Westwater, 1983: A steerable dual-channel microwave radiometer for measurement of water vapor and liquid in the troposphere. *J. Appl. Meteor.*, **22**, 789–806.

Houze, Jr, R. A., S. A. Rutledge, T. J. Matejka, and P. V. Hobbs, 1981: The mesoscale and microscale structure and organization of clouds and precipitation in midlatitude cyclones. III: Air motions and precipitation growth in a warm-frontal rainband. *J. Atmos. Sci.*, **38**, 639–649.

Kessler, E., 1969: *On the Distribution and Continuity of Water Substance in Atmospheric Circulations. Meteor. Monogr.,* No. 32, Amer. Meteor. Soc., 84 pp.

Khairoutdinov, M., and Y. Kogan, 2000: A new cloud physics parameterization in a large-eddy simulation model of marine stratocumulus. *Mon. Wea. Rev.*, **128**, 229–243.

_____, and D. A. Randall, 2001: A cloud-resolving model as a cloud parameterization in the NCAR Community Climate System Model: Preliminary results. *Geophys. Res. Lett.*, **28**, 3617-3620.

Khvorostyanov, V. I., and J. A. Curry, 2002: Terminal velocities of droplets and crystals: Power laws with continuous parameters over the size spectrum. *J. Atmos. Sci.*, **59**, 1872–1884.

Lawson, R. P., and T. L. Jensen, 1998: Improved microphysical observations in mixed phase clouds. *Conf. On Cloud Physics*, Everett, WA, Amer. Meteor. Soc., 451-454.

_____, R. E. Stewart, J. W. Strapp, and G. A. Isaac, 1993: Aircraft observations of the origin and growth of very large snowflakes. *Geophys. Res. Lett.*, **20**, 53-56.

_____, _____, and L. J. Angus, 1998: Observations and numerical simulations of the origin and development of very large snowflakes. *J. Atmos. Sci*., **55**, 3209–3229.

Lin, Y.-L., R. D. Farley, and H. D. Orville, 1983: Bulk parameterization of the snow field in a cloud model. *J. Clim. Appl. Meteorol.*, **22**, 1065-1092.

Locatelli, J. D., and P. V. Hobbs, 1974: Fall speeds and masses of solid precipitation particles. *J. Geophys. Res.*, **79**, 2185–2197.

Magono, C., and C. W. Lee, 1966: Meteorological classification of natural snow crystals. *J. Faculty of Science, Hokkaido Univ., Series VII*, **2**, 321-335.

Manning, K. W., and C. A. Davis, 1997: Verification and sensitivity experiments for the WISP94 MM5 forecasts. *Wea. Forecasting*, **12**, 719–735.

Manton, M. J., and W. R. Cotton, 1977: Parameterization of the atmospheric surface layer. *J. Atmos. Sci.,* **34,** 331–334.

Mass, C. F., D. Ovens, K. Westrick, and B. A. Colle, 2002: Does increasing horizontal resolution produce more skillful forecasts? *Bull. Amer. Meteor. Soc.*, **83**, 407–430.

Mitchell, D. L., 1996: Use of mass- and area-dimensional power laws for determining precipitation particle terminal velocities. *J. Atmos. Sci*., **53**, 1710–1723.

Meyers, M. P., P. J. DeMott, and W. R. Cotton, 1992: New primary ice-nucleation parameterizations in an explicit cloud model. *J. Appl. Meteor.,* **31,** 708–721.

Mossop, S. C., 1985: The microphysical properties of supercooled cumulus clouds in which an ice particle multiplication process operated. *Quart. J. Roy. Meteor. Soc.,* **111,** 183–198.

Olson, D. A., N. W. Junker, and B. Korty, 1995: Evaluation of 33 years of quantitative precipitation forecasting at the NMC. *Wea. Forecasting*, **10**, 498–511.

Rangno, A. L., and P. V. Hobbs, 1991: Ice particle concentrations and precipitation development in small polar maritime cumuliform clouds. *Quart. J. Roy. Meteor. Soc.,* **117,** 207–241.

——, and ——, 1994: Ice particle concentrations and precipitation development in small continental cumuliform clouds. *Quart. J. Roy. Meteor. Soc.,* **120,** 573–601.

Rasmussen, R., and co-authors, 1992: Winter Icing and Storms Project (WISP). *Bull. Amer. Meteor. Soc*., **73**, 951-974.

——, J. Vivekanandan, J. Cole, B. Myers, and C. Masters, 1999: The estimation of snowfall rate using visibility. *J. Appl. Meteor*., **38**, 1542–1563.

——, I. Geresdi, G. Thompson, K. Manning, and E. Karplus, 2002: Freezing drizzle formation in stably stratified layer clouds: The role of radiative cooling of cloud droplets, cloud condensation nuclei, and ice initiation. *J. Atmos. Sci*., **59**, 837–860.

Reinking, R. F., J. B. Snider, and J. L. Coen, 2000: Influences of storm-embedded orographic gravity waves on cloud liquid water and precipitation. *J. Appl. Meteorol.*, **39**, 733–759.

Reisner, J., R. M. Rasmussen, and R. T. Bruintjes, 1998: Explicit forecasting of supercooled liquid water in winter storms using the MM5 mesoscale model. *Quart. J. Roy. Meteor. Soc.*, **124**, 1071-1107.

Reynolds, D. W., and A. S. Dennis, 1986: Review of the Sierra Cooperative Pilot Project. *Bull. Amer. Meteor. Soc.*, **67**, 513-523.

Rutledge, S. A., and P. V. Hobbs, 1983: The mesoscale and microscale structure and organization of clouds and precipitation in midlatitude cyclones. VIII. A model for the "seeder-feeder" process in warm-frontal rainbands. *J. Atmos. Sci.*, **40**, 1185–1206.

_____, and _____, 1984: The mesoscale and microscale structure and organization of clouds and precipitation in mid-latitude cyclone. XII: A diagnostic modeling study of precipitation development in narrow cold-frontal rainbands. *J. Atmos. Sci.*, **41**, 2949–2972.

Straka, J. M., and E. N. Rasmussen, 1997: Toward improving microphysical parameterizations of conversion processes. *J. Appl. Meteor.,* **36,** 896–902

Telford, J. W., and P. B. Wagner, 1981: Observations of condensation growth determined by entity type mixing. *Pure Appl. Geophys.,* **119,** 934–965.

Vivekanandan, J., D. S. Zrnic, S. M. Ellis, R. Oye, A. V. Ryzhkov, and J. Straka, 1999: Cloud microphysics retrieval using S-band dual-polarization radar measurements. *Bull. Amer. Meteor. Soc.,* **80**, 381–388.

Westrick, K. J., and C. F. Mass, 2001: An evaluation of a high-resolution hydrometeorological modeling system for prediction of a cool-season flood event in a coastal mountainous watershed. *J. Hydrometeor.,* **2**, 161–180.

Wurman, J., 1994: Vector winds from a single-transmitter bistatic dual-Doppler radar network. *Bull. Amer. Meteor. Soc*., **75**, 983–994.

_____, S. Heckman, and D. Boccippio, 1993: A bistatic multiple-Doppler network. *J. Appl. Meteor.*, **32**, 1802–1814.

Zikmunda, J., and G. Vali, 1972: Fall patterns and fall velocities of rimed ice crystals. *J. Atmos. Sci.,* **29**, 1334–1347.

FIGURE CAPTIONS

FIG. 1. The 24-h bias scores for the 36-, 12-, and 4-km domains of the University of Washington's Pacific Northwest MM5 model forecasts from 1 January 1998 through 15 March 1998 and 1 October 1998 through 8 March 1999. From Colle et al. (2000).

FIG. 2. Map of Pacific Northwest region, showing locations of the Frontal and Orographic Study Areas (heavy blue outlines), the University of Washington, Paine Field, and NWS rawinsonde and WSR-88D radar sites.

FIG. 3. Map of the IMPROVE-1 Frontal Study Area, showing locations of observational facilities.

FIG. 4. Map of the IMPROVE-2 Orographic Study Area, showing locations of observational facilities.

FIG. 5. Size ranges for cloud and precipitation size spectra measurements and imagery from instruments aboard the UW Convair-580 research aircraft.

FIG. 6. Flight strategies employed during IMPROVE-1 (left panels) and IMPROVE-2 (right panels). Top panels show plan view and bottom panels show vertical cross sections. Dark blue lines are UW Convair-580 flight tracks, green and red lines are NOAA P-3 flight tracks. The temperatures indicated in the lower panels are typical for the indicated heights in the Pacific Northwest in winter.

FIG. 7. IMPROVE operations. Top row (left to right): Media personnel report on IMPROVE-1 operations at the NCAR S-Pol radar control trailer; NOAA P-3 flight scientist

communicates with the radar scientist on the ground during an IMPROVE-2 research flight; local school children visit the NCAR S-Pol radar site for a tutorial during IMPROVE-1. Second row: The UW Convair-580 research aircraft passes over the Seattle area en route to the IMPROVE-1 Frontal Study Area; UW Convair-580 science and flight crew members investigate possible damage from an in-flight lightning strike after the final IMPROVE-1 research flight; PNNL scientists at the PARSL site in Sisters, Oregon, during IMPROVE-2. Third row: a sonde is launched from the mobile UW sonde trailer during IMPROVE-2; the NOAA/ETL S-band profiler at McKenzie Bridge, Oregon; gathering of snow crystals near Santiam Pass, Oregon, during IMPROVE-2. Bottom row: radar scientists examine real-time radar displays and communicate with the research aircraft from the S-Pol radar trailer during IMPROVE-2; a U.S. Navy visitor holds the ice cap that accumulated on the nose of the NOAA P-3 during heavy icing conditions on an IMPROVE-2 research flight; the S-Pol radar site in IMPROVE-1, at the South Jetty in Westport, Washington.

FIG. 8. Time series of precipitation accumulations at special raingauge sites at (a) Kalaloch, Washington, during IMPROVE-1, and (b) Falls Creek, Oregon, during IMPROVE-2. Blue bands show time periods of IMPROVE IOPs. Date hash marks are at 12:01 AM local time. See Figs. 2 and 3 for locations.

FIG. 9. Infrared satellite image, with NCEP-analyzed fronts overlaid, at 0000 UTC 2 February 2001.

FIG. 10. Time-height cross section of onshore frontal passage on 1-2 February 2001, based on special IMPROVE soundings at Quillayute and Westport, Washington. Red contours show potential temperature every 2 K, blue contours show equivalent potential temperature every 4 K. Solid black lines are frontal boundaries, and green shaded area shows the time period and

vertical extent of precipitation associated with the upper cold-frontal rainband, as determined from S-Pol radar scans.

FIG. 11. RHI radar scans along the 240^{O} azimuth at (a) 0054 UTC and (b) 0125 UTC 2 February 2001, showing generating cells and fallstreaks in the eastern-most (right-most) part of the upper-cold-frontal rainband. Two layers of generating cells are indicated: the cirrus layer of generating cells (labeled "Ci"), and the altocumulus layer of generating cells (labeled "Ac").

FIG. 12. Vertical cross section through the upper cold-frontal rainband of 1-2 February 2001. Color shades are the polarimetric particle identification result from an RHI scan of the NCAR S-Pol radar along the 250^{O} azimuth at 0156 UTC 2 February 2001. Color code is shown at top. The magenta-colored clutter signal of the UW Convair-580 research aircraft can be seen immediately in front of the aircraft symbol. The black line shows the entire aircraft flight track in a reference frame moving with the rainband. Shown at left are several images of ice crystals that were recorded by the Cloud Particle Imager on the aircraft in the altitude ranges indicated by the brackets.

FIG. 13. Infrared satellite image, with NCEP-analyzed fronts overlaid, at 0000 UTC 14 December 2001.

FIG. 14. Time series of vertically integrated liquid water content (LWC) measured with a ground-based microwave radiometer (see Fig. 3 for location of radiometer) on 13-14 December 2001.

FIG. 15. Sample imagery from the PMS 2D-C probe aboard the UW Convair-580 aircraft on 13-14 December 2001. Solid line with arrow heads shows flight track. The sample particle images were observed at the points indicated by the blue arrows. The region of ice phase

precipitation is indicated by gray fallstreaks, and the top of the cloud liquid water region is indicated by the gray scalloped cloud outline. Height is indicated on left axis and temperature is indicated by the labeled horizontal line segments.

FIG. 16. Polarimetric particle identification result from an RHI scan of the NCAR S-Pol radar along the 85^{O} azimuth at 0003 UTC 14 December 2001. Color code for particle type is shown at right.

FIG. 17. Time-height cross sections of measurements from the S-band profiler (see Fig. 3 for location) on 14 Dec 2001. (a) Reflectivity. (b) Doppler vertical velocity. Height is above sea-level, times are in UTC, and positive velocity values are downward.

FIG. 18. Cross sections through precipitation events simulated by the MM5 model on (a) 1-2 February 2001, and (b) 13-14 December 2001. Shading indicates equivalent potential temperature (θe), with key given at right. Thin black lines are temperature in ºC. Hydrometeor mixing ratios are indicated by contour types as follows: cloud water, solid white; rain, dashed white; snow, short-dashed black; and graupel, dash-dot black. Contour values in (a) are 0.1 g kg^{-1} for all types, and a second contour of 0.3 g kg^{-1} for cloud water and snow. Contour values in (b) are 0.2 g kg^{-1} for all types, and a second contour of 1.0 g kg^{-1} for cloud water and graupel. Regions covered by the UW Convair-580 flights are indicated by an aircraft symbol and large bracket.

FIG. 19. Precipitation accumulated during the period 1400 UTC 13 December 2002—0800 UTC 14 December 2002 from a 4-km MM5 model simulation, expressed as a percentage of observed precipitation at raingauge sites in the vicinity of the IMPROVE-2 study area. Terrain heights shown at lower left, and color coding of percentage ranges shown at upper left.

TABLE 1. Instrument platforms deployed during the two IMPROVE field studies.

Instrument Platform	**Source***
UW Convair-580 research aircraft [1,2]	UW
NOAA P-3 research aircraft [2]	NOAA/AOC
NCAR S-Pol radar [1,2]	NCAR/ATD
NCAR bistatic network (BINET) receivers [1]	NCAR/ATD
Ground-based snow crystal observations [2]	UW
NCAR integrated sounding systems (ISS) [2]	NCAR/ATD
ETL S-band profiler [2]	NOAA/ETL
ETL wind profilers [1,2]	NOAA/ETL
Special NWS rawinsondes [1,2]	NOAA/NWS
Special rawinsondes [1,2]	UW, U.S. Navy, PNNL, NCAR/RAP
NCAR scanning microwave radiometer [1,2]	NCAR/ATD
UW raingauge network [1,2]	UW
UW disdrometer [2]	UW
PNNL remote sensing laboratory (PARSL) [1,2]	PNNL

* UW: University of Washington; NOAA: National Oceanographic and Atmospheric Administration; AOC: Aircraft Operations Center; NCAR: National Center for Atmospheric Research; ATD: Atmospheric Technology Division; ETL: Environmental Technology Laboratory; NWS: National Weather Service; PNNL: Pacific Northwest National Laboratory; RAP: Research Applications Program.

[1] Operated during IMPROVE-1.

[2] Operated during IMPROVE-2.

TABLE 2. Intensive observing periods (IOP) carried out during IMPROVE-1.

IOP Number	**Date (2001)**	**Types of frontal rainbands studied**
1	4 Jan	Warm-sector rainbands and cold-frontal rainband
2	7 Jan	Upper cold-frontal rainband
3	9 Jan	Upper cold-frontal and occluded-frontal rainbands
4	12 Jan	Upper cold-frontal rainband
5	18 Jan	Warm-frontal and occluded-frontal rainbands
6	20 Jan	Occluded-frontal rainband and warm-frontal rainband
7	23 Jan	Rainbands associated with a cut-off low
8	28 Jan	Two prefrontal rainbands and a narrow cold-frontal rainband
9	1 Feb	Upper cold-frontal rainband
10	8 Feb	Warm-frontal and cold-frontal rainbands
11	10 Feb	Narrow and wide cold-frontal rainbands

TABLE 3. Intensive observing periods (IOP) carried out during IMPROVE-2.

IOP Number	**Date (2001)**	**Types of orographic precipitation studied**
1	28 Nov	Occluded-frontal band over mountains
2	29 Nov	Postfrontal cross-barrier flow forcing shallow orographic precipitation
3	1 Dec	Postfrontal cross-barrier flow forcing deep orographic precipitation
4	4 Dec	Postfrontal cross-barrier flow forcing deepening orographic precipitation
5	5 Dec	Passage of upper cold-frontal and occluded-frontal bands over mountains
6	6 Dec	Postfrontal cross-barrier flow forcing deep orographic precipitation
7	8 Dec	Passage of two cold-frontal rainbands over mountains
8	11 Dec	Postfrontal cross-barrier flow forcing shallow orographic precipitation
9	12 Dec	Warm-advection cross-barrier flow with two embedded rainbands
10	13 Dec	Passage of upper cold-frontal and occluded-frontal bands over mountains
11	15 Dec	Warm-advection cross-barrier flow forcing cellular orographic precipitation
12	16 Dec	Warm-advection prefrontal precipitation, then narrow cold-frontal band
13	18 Dec	Passage of pre-frontal band and post-frontal comma cloud over mountains
14	19 Dec	Passage of warm-frontal band (perpendicular to ridge) over mountains
15	22 Dec	Narrow cold-frontal band dissipating as it passed over mountains

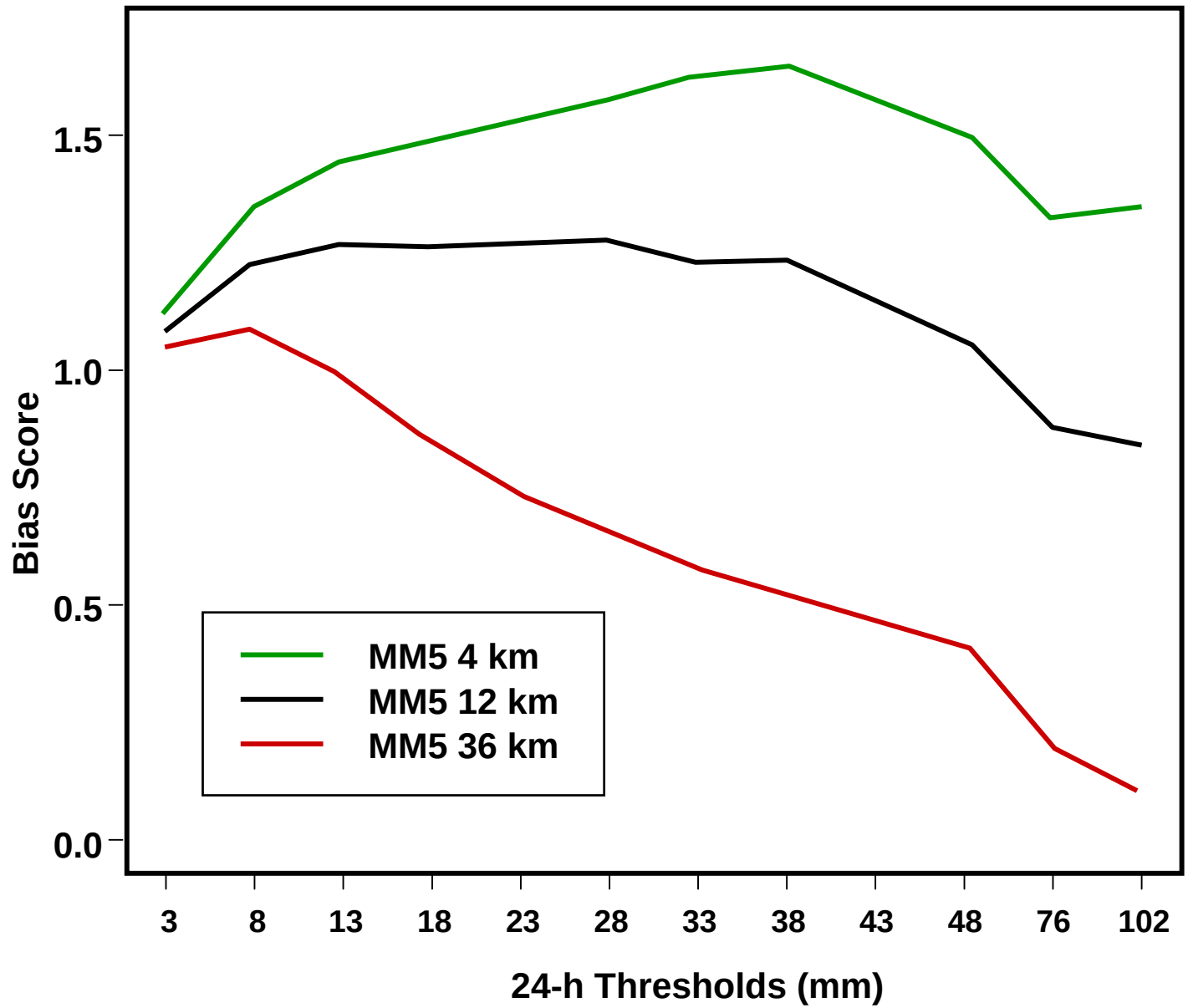

Stoelinga et al. Fig. 1. The 24-h bias scores for the 36-, 12-, and 4-km domains of the University of Washington's Pacific Northwest MM5 model forecasts from 1 January 1998 through 15 March 1998 and 1 October 1998 through 8 March 1999. From Colle et al. (2000).

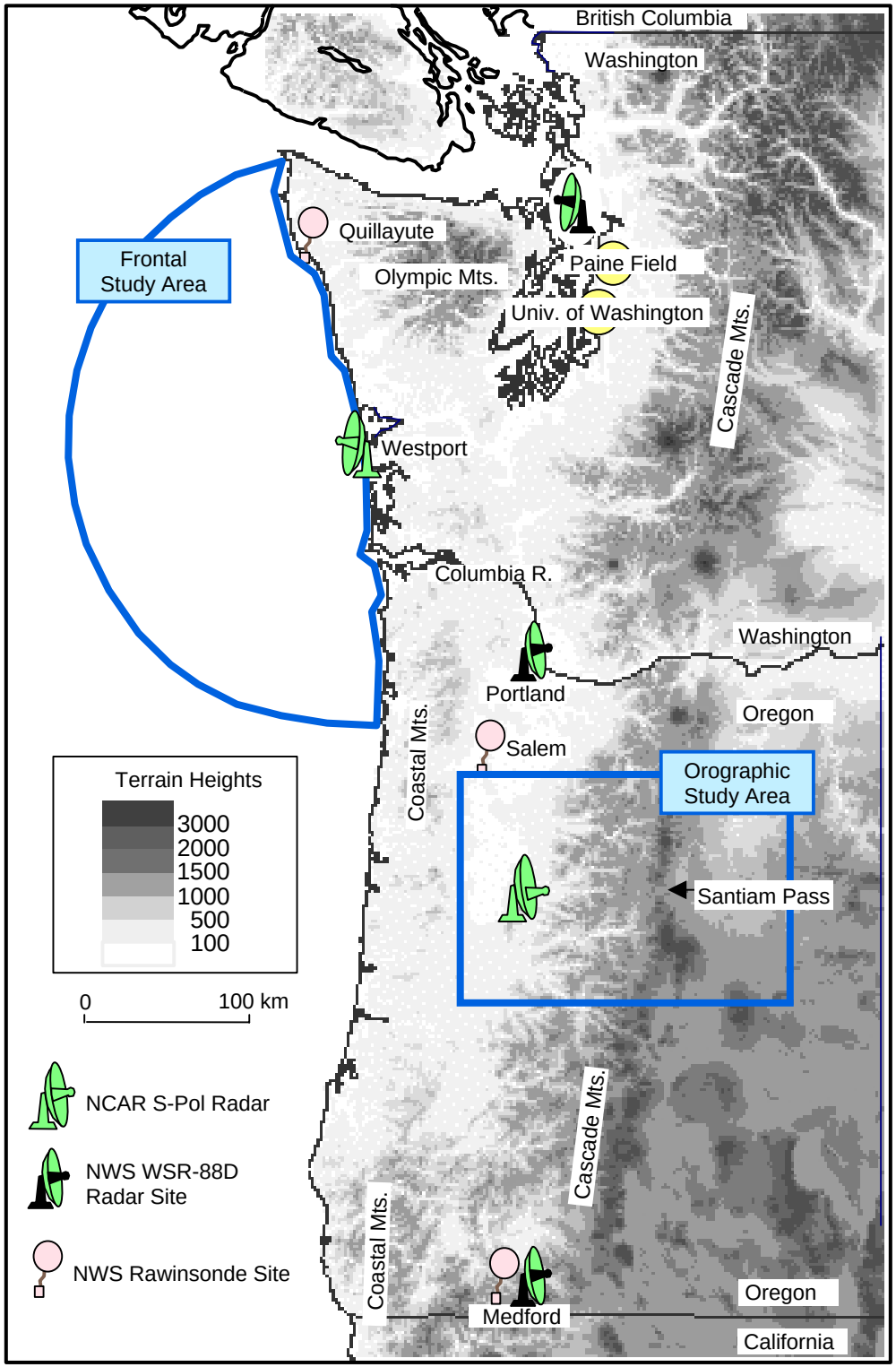

Stoelinga et al. Fig. 2. Map of Pacific Northwest region, showing locations of the Frontal and Orographic Study Areas (heavy blue outlines), the University of Washington, Paine Field, and NWS rawinsonde and WSR-88D radar sites.

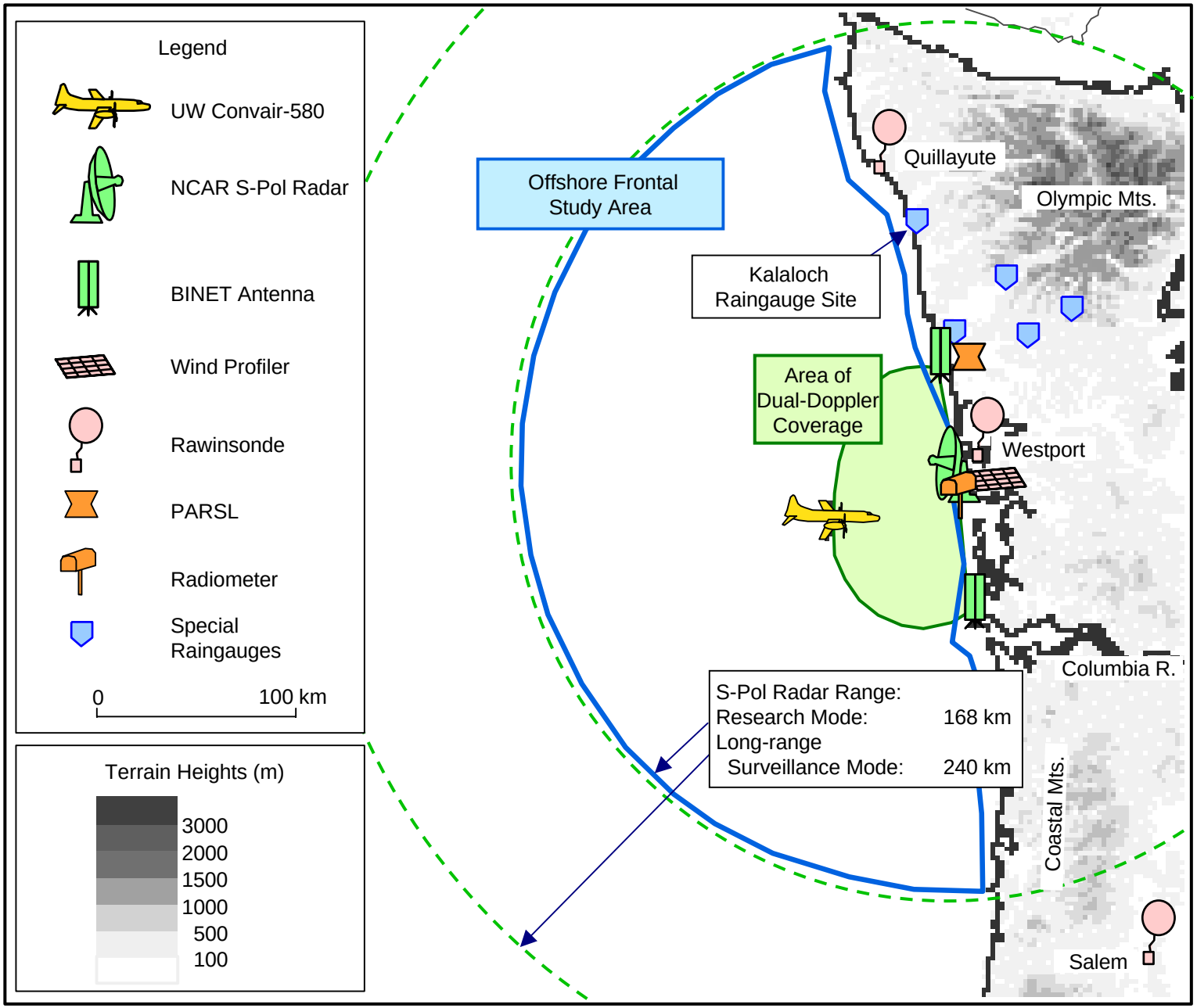

Stoelinga et al. Fig. 3. Map of the IMPROVE-1 Frontal Study Area, showing locations of observational facilities.

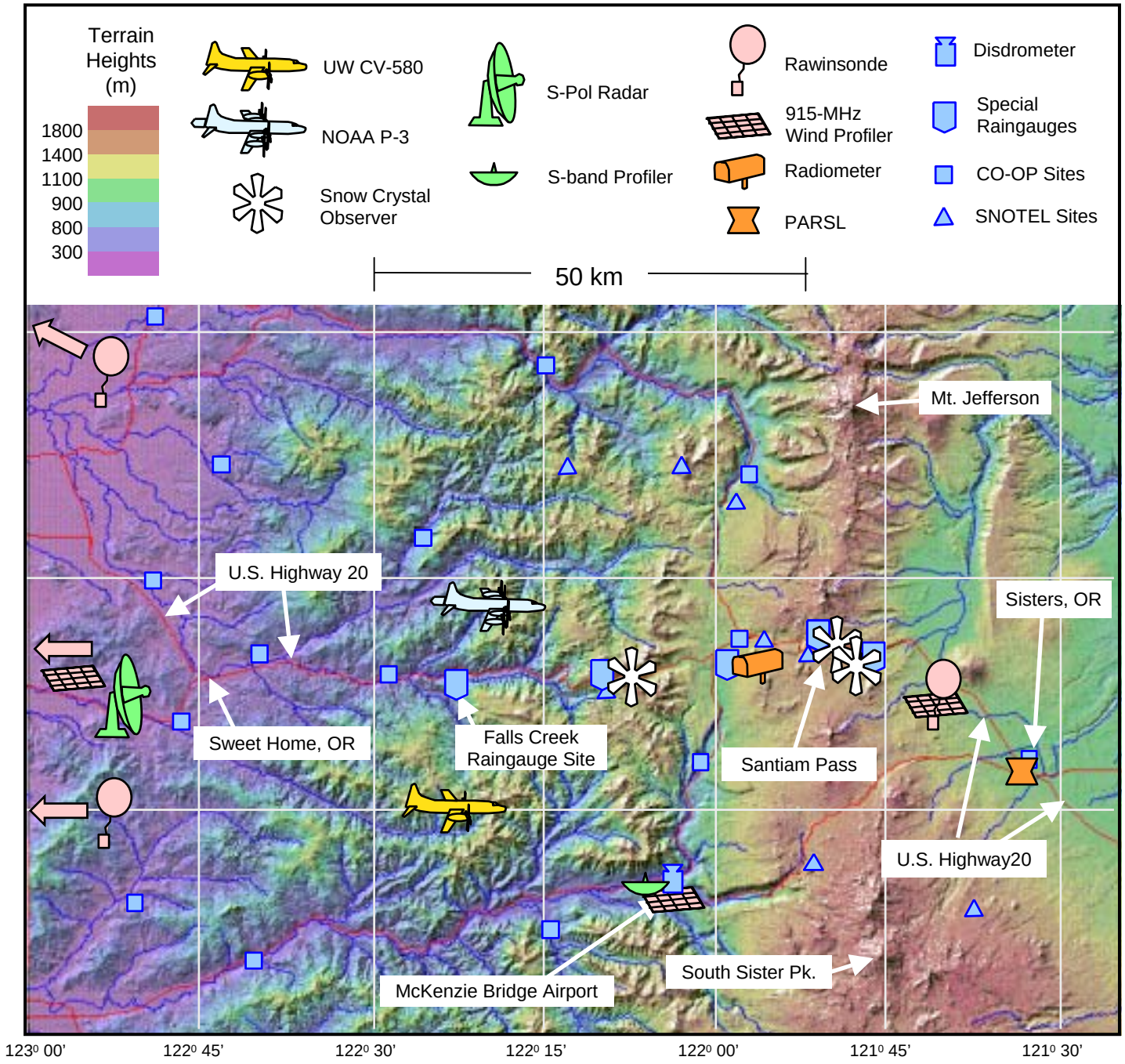

Stoelinga et al. Fig. 4. Map of the IMPROVE-2 Orographic Study Area, showing locations of observational facilities.

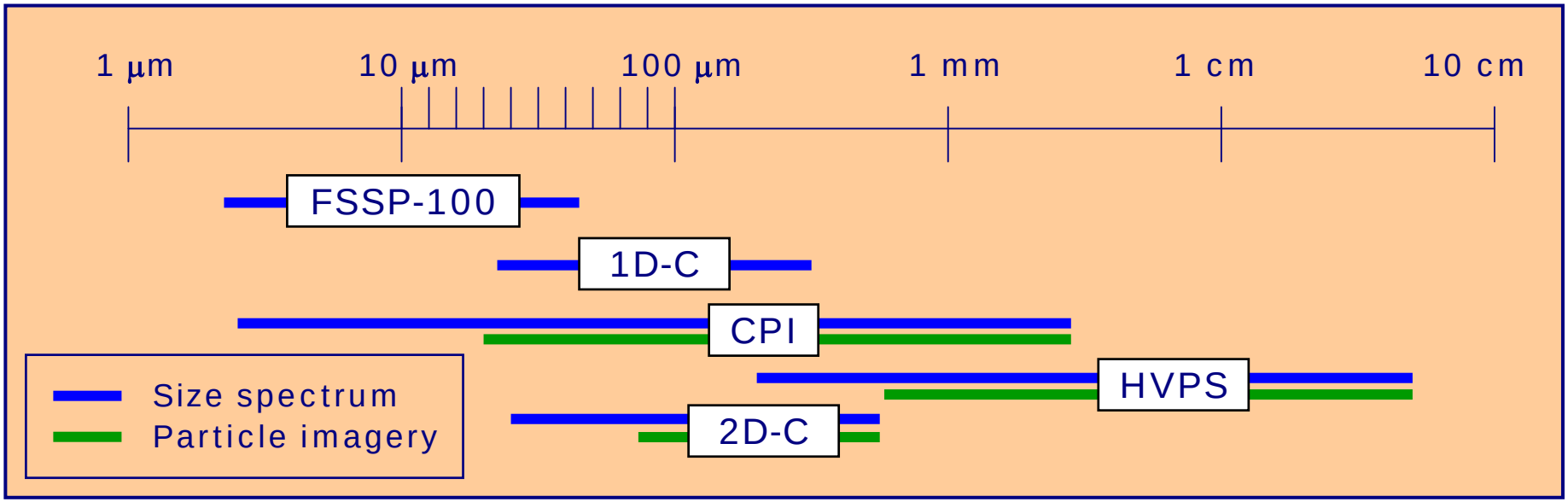

Stoelinga et al. Fig. 5. Size ranges for cloud and precipitation size spectra measurements and imagery from instruments aboard the UW Convair-580 research aircraft.

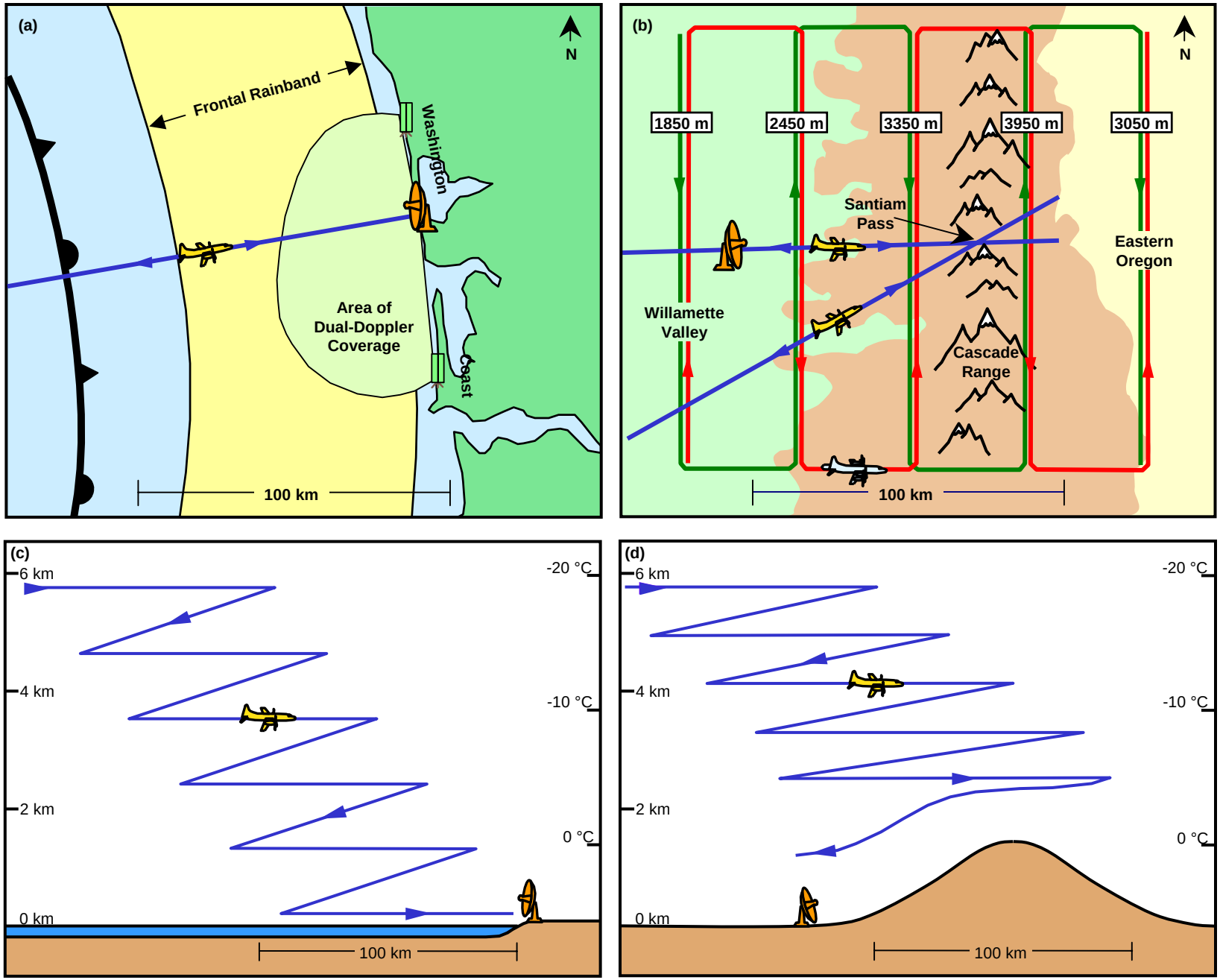

Stoelinga et al. Fig. 6. Flight strategies employed during IMPROVE-1 (left panels) and IMPROVE-2 (right panels). Top panels show plan view and bottom panels show vertical cross sections. Dark blue lines are UW Convair-580 flight tracks, green and red lines are NOAA P-3 flight tracks. The temperatures indicated in the lower panels are typical for the indicated heights in the Pacific Northwest in winter.

Stoelinga et al. Fig. 7. IMPROVE operations. Top row (left to right): Media personnel report on IMPROVE-1 operations at the NCAR S-Pol radar control trailer; NOAA P-3 flight scientist communicates with the radar scientist on the ground during an IMPROVE-2 research flight; local school children visit the NCAR S-Pol radar site for a tutorial during IMPROVE-1. Second row: The UW Convair-580 research aircraft passes over the Seattle area en route to the IMPROVE-1 Frontal Study Area; UW Convair-580 science and flight crew members investigate possible damage from an in-flight lightning strike after the final IMPROVE-1 research flight; PNNL scientists at the PARSL site in Sisters, Oregon, during IMPROVE-2. Third row: a sonde is launched from the mobile UW sonde trailer during IMPROVE-2; the NOAA/ETL S-band profiler at McKenzie Bridge, Oregon; gathering of snow crystals near Santiam Pass, Oregon, during IMPROVE-2. Bottom row: radar scientists examine real-time radar displays and communicate with the research aircraft from the S-Pol radar trailer during IMPROVE-2; a U.S. Navy visitor holds the ice cap that accumulated on the nose of the NOAA P-3 during heavy icing conditions on an IMPROVE-2 research flight; the S-Pol radar site in IMPROVE-1, at the South Jetty in Westport, Washington.

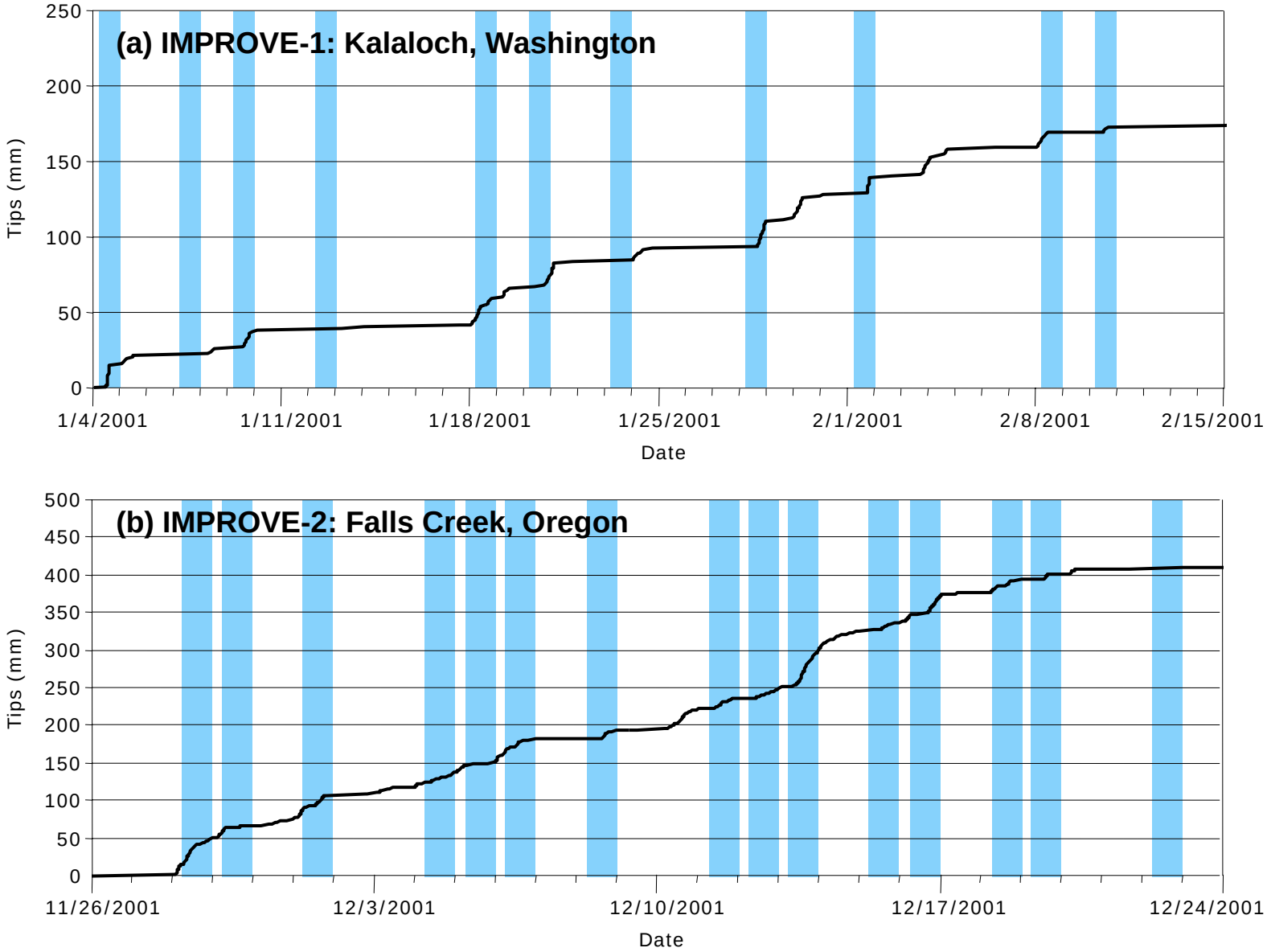

Stoelinga et al. Fig. 8. Time series of precipitation accumulations at special raingauge sites at (a) Kalaloch, Washington, during IMPROVE-1, and (b) Falls Creek, Oregon, during IMPROVE-2. Blue bands show time periods of IMPROVE IOPs. Date hash marks are at 12:01 AM local time. See Figs. 2 and 3 for locations.

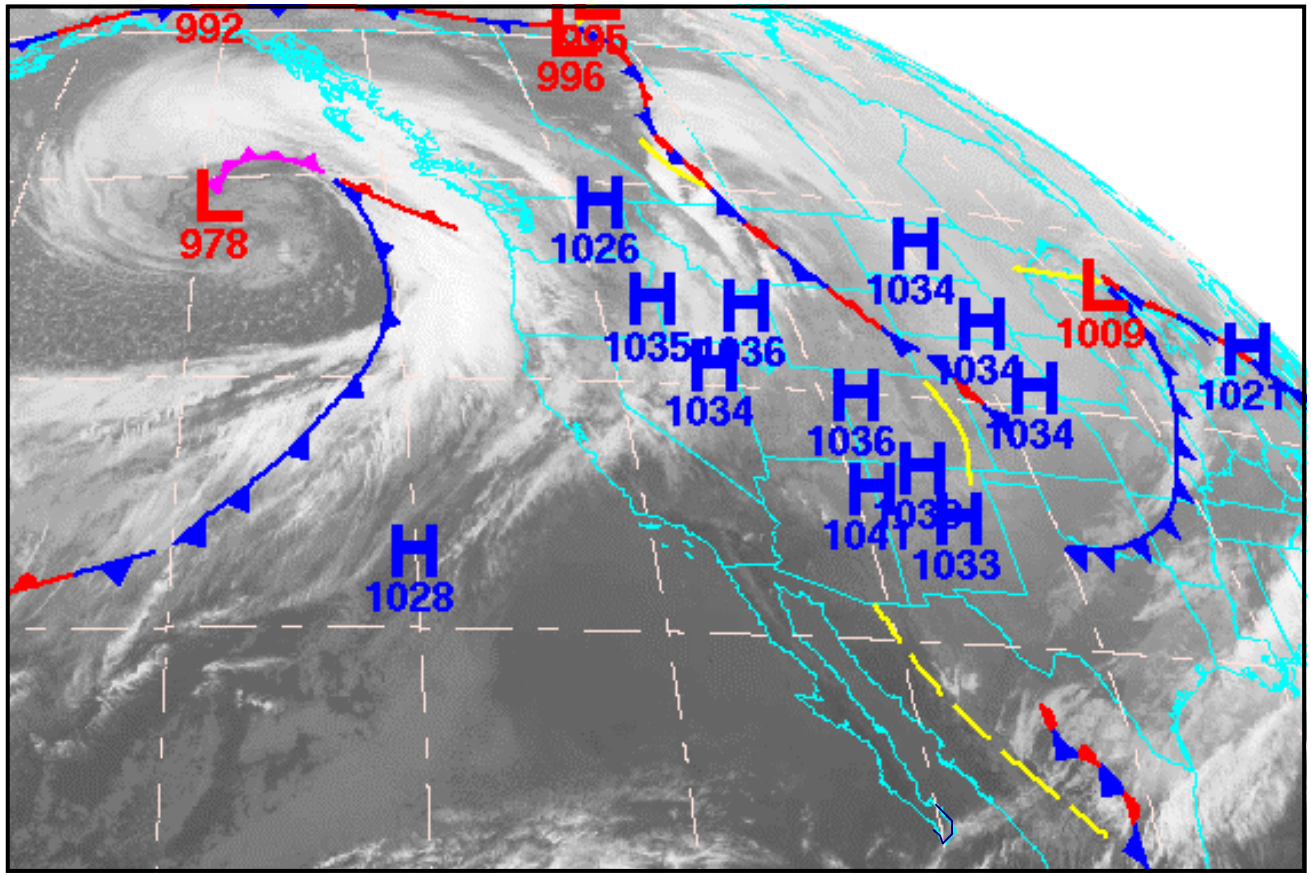

Stoelinga et al. Fig. 9. Infrared satellite image, with NCEP-analyzed fronts overlaid, at 0000 UTC 2 February 2001.

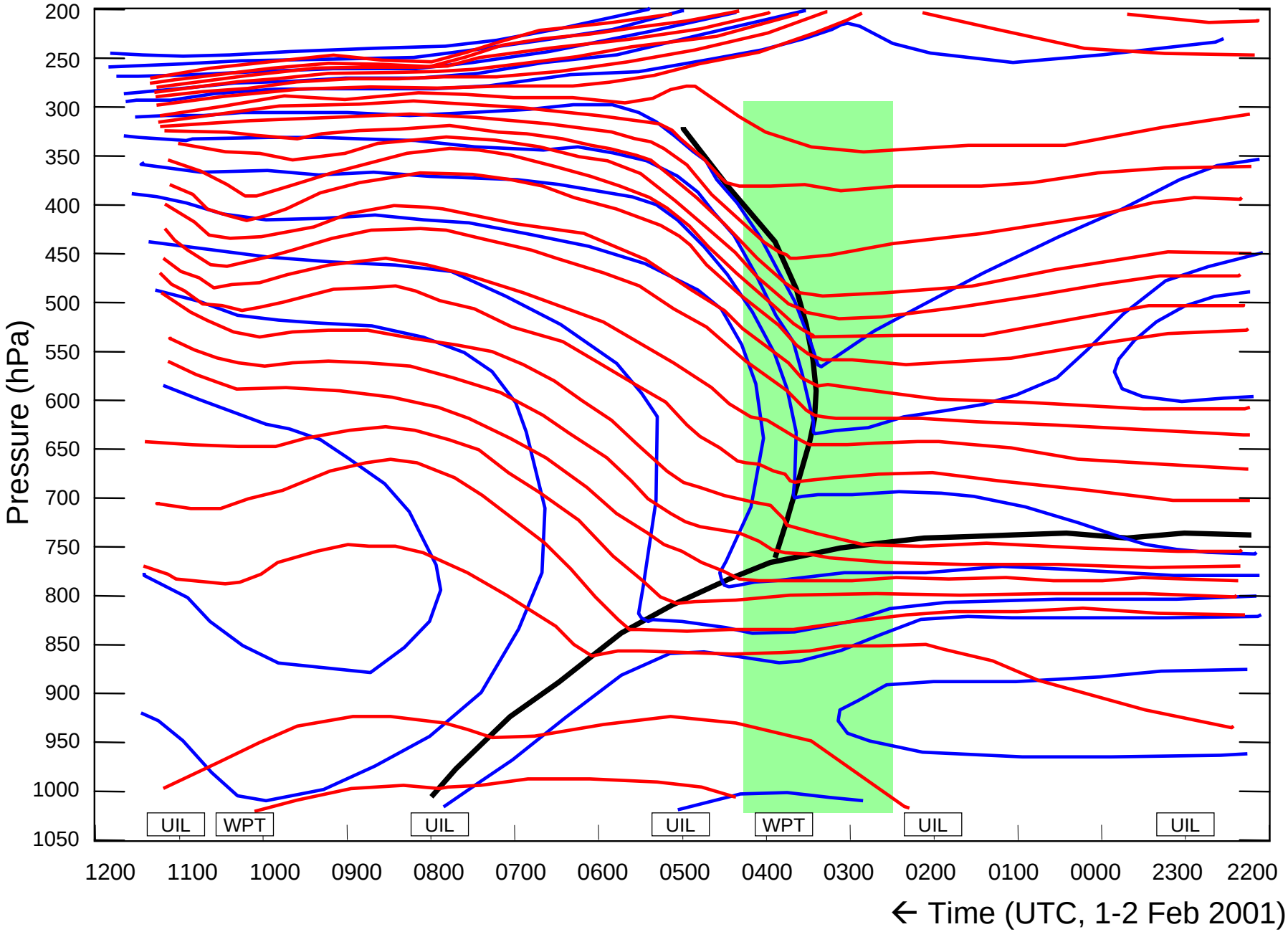

Stoelinga et al. Fig. 10. Time-height cross section of onshore frontal passage on 1-2 February 2001, based on special IMPROVE soundings at Quillayute and Westport, Washington. Red contours show potential temperature every 2 K, blue contours show equivalent potential temperature every 4 K. Solid black lines are frontal boundaries, and green shaded area shows the time period and vertical extent of precipitation associated with the upper cold-frontal rainband, as determined from S-Pol radar scans.

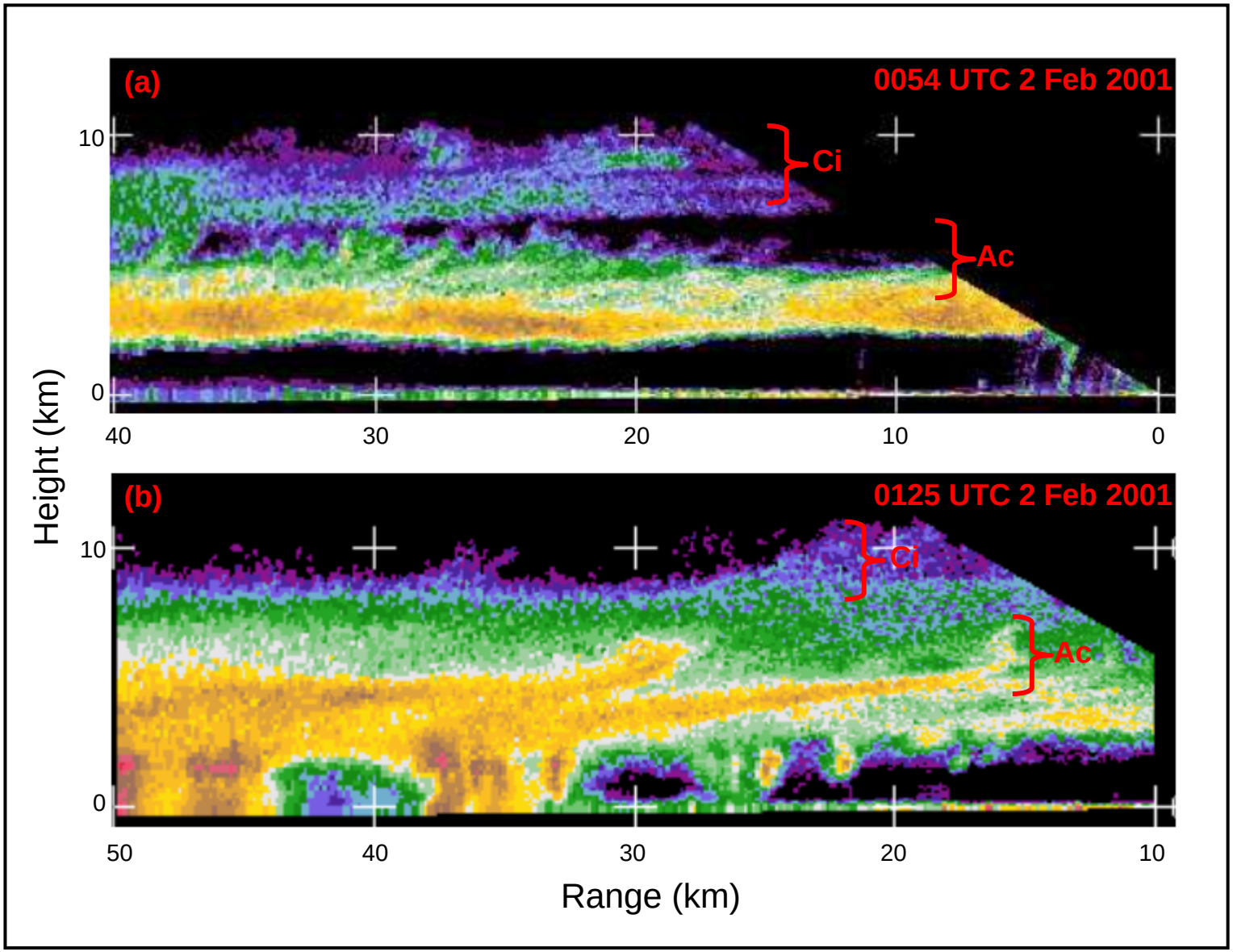

Stoelinga et al. Fig. 11. RHI radar scans along the 240^{O} azimuth at (a) 0054 UTC and (b) 0125 UTC 2 February 2001, showing generating cells and fallstreaks in the eastern-most (right-most) part of the upper-cold-frontal rainband. Two layers of generating cells are indicated: the cirrus layer of generating cells (labeled “Ci”), and the altocumulus layer of generating cells (labeled “Ac”).

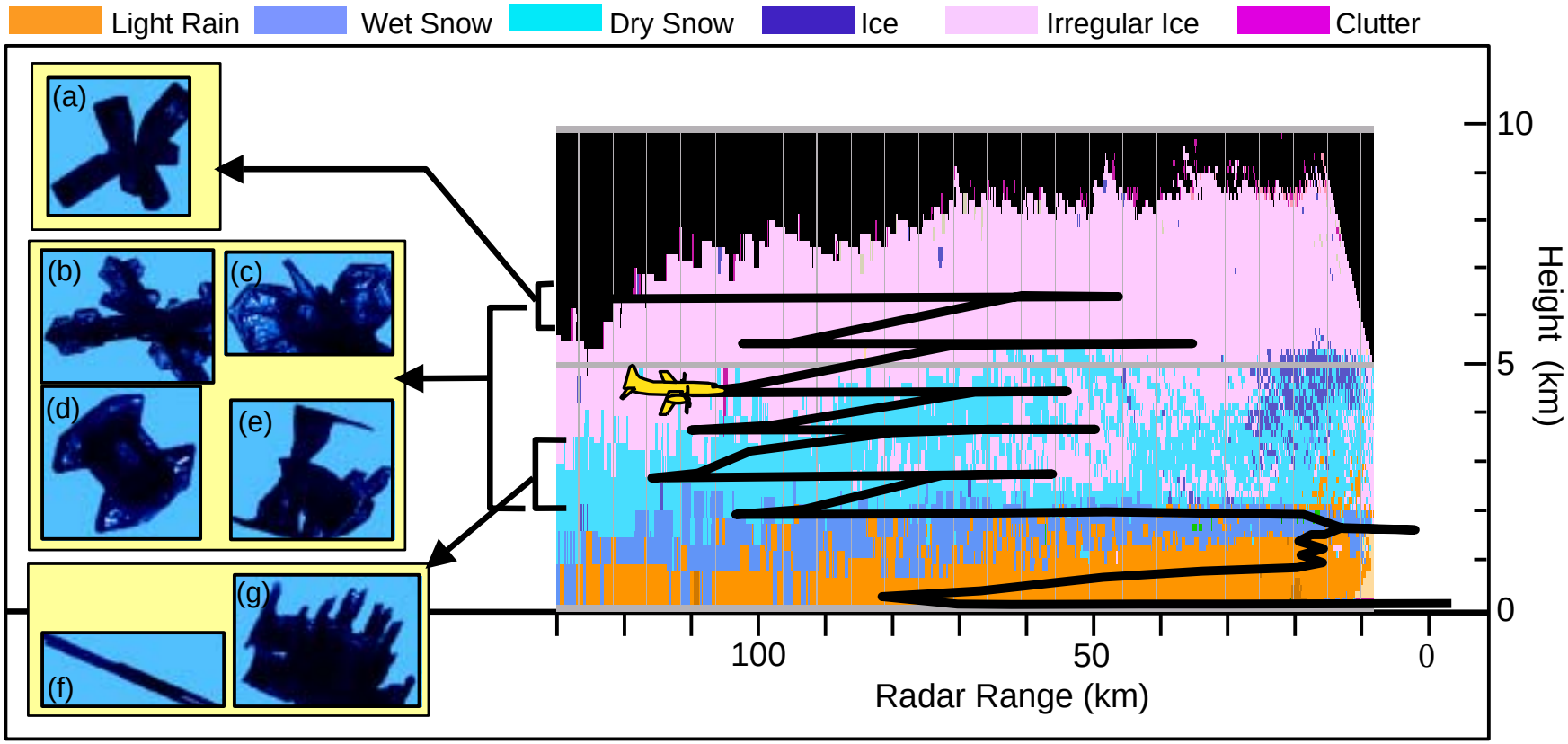

Stoelinga et al. Fig. 12. Vertical cross section through the upper cold-frontal rainband of 1-2 February 2001. Color shades are the polarimetric particle identification result from an RHI scan of the NCAR S-Pol radar along the 250^{O} azimuth at 0156 UTC 2 February 2001. Color code is shown at top. The magenta-colored clutter signal of the UW Convair-580 research aircraft can be seen immediately in front of the aircraft symbol. The black line shows the entire aircraft flight track in a reference frame moving with the rainband. Shown at left are several images of ice crystals that were recorded by the Cloud Particle Imager on the aircraft in the altitude ranges indicated by the brackets.

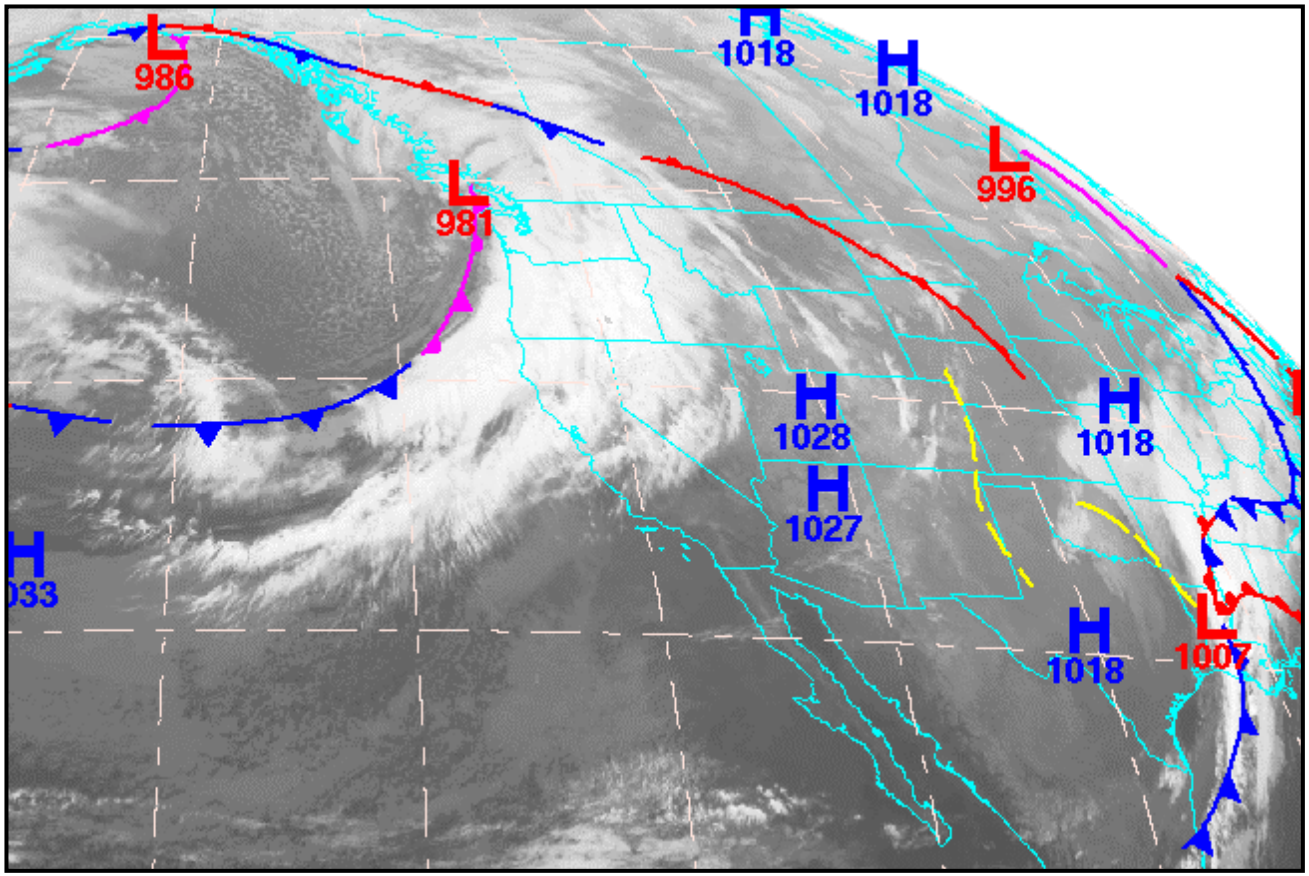

Stoelinga et al. Fig. 13. Infrared satellite image, with NCEP-analyzed fronts overlaid, at 0000 UTC 14 December 2001.

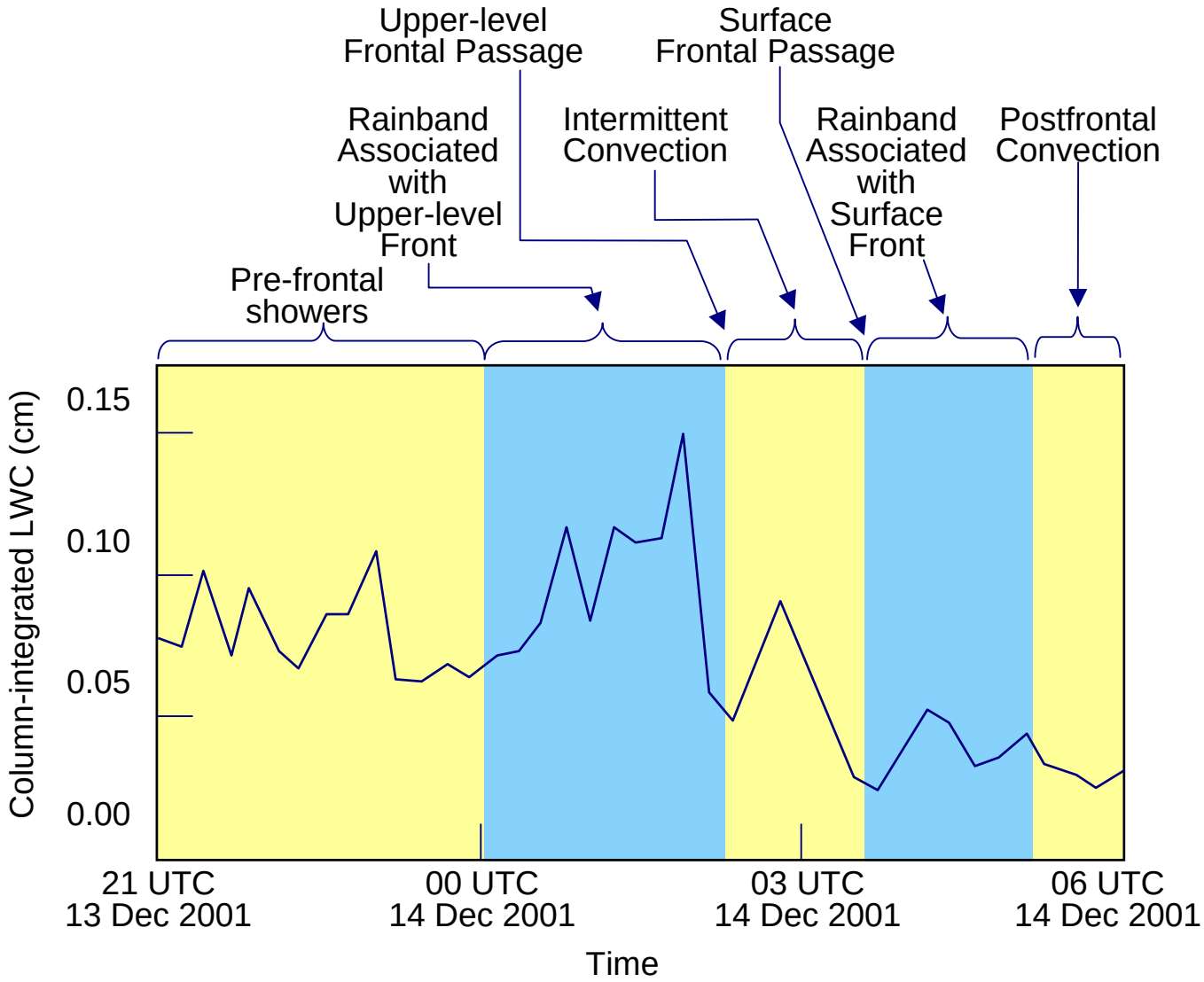

Stoelinga et al. Fig. 14. Time series of vertically integrated liquid water content (LWC) measured with a ground-based microwave radiometer (see Fig. 3 for location of radiometer) on 13-14 December 2001.

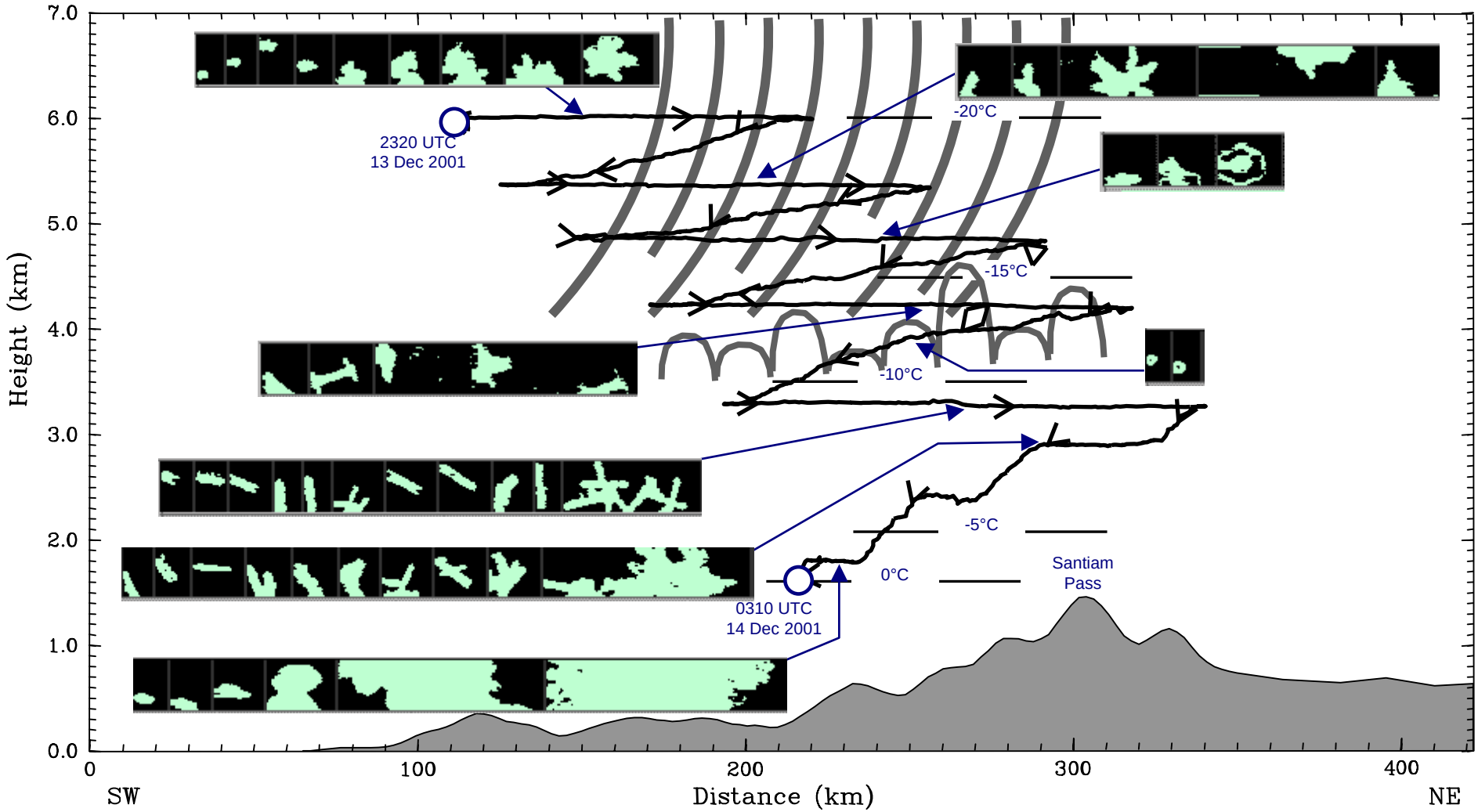

Stoelinga et al. Fig. 15. Sample imagery from the PMS 2D-C probe aboard the UW Convair-580 aircraft on 13-14 December 2001. Solid line with arrow heads shows flight track. The sample particle images were observed at the points indicated by the blue arrows. The region of ice phase precipitation is indicated by gray fallstreaks, and the top of the cloud liquid water region is indicated by the gray scalloped cloud outline. Height is indicated on left axis and temperature is indicated by the labeled horizontal line segments.

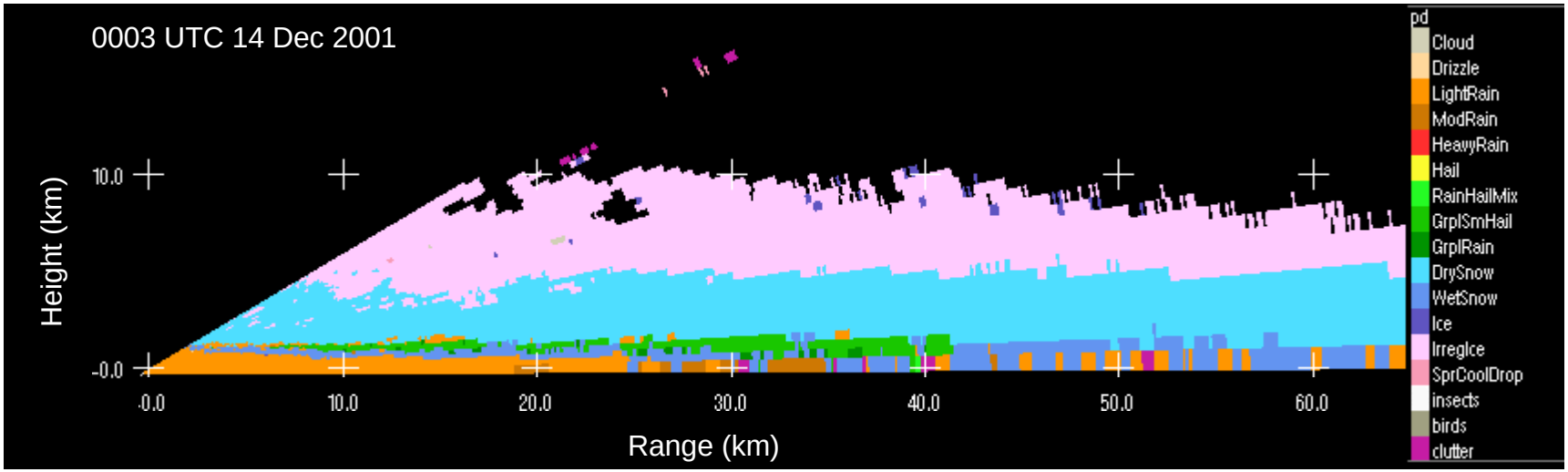

Stoelinga et al. Fig. 16. Polarimetric particle identification result from an RHI scan of the NCAR S-Pol radar along the 85^{O} azimuth at 0003 UTC 14 December 2001. Color code for particle type is shown at right.

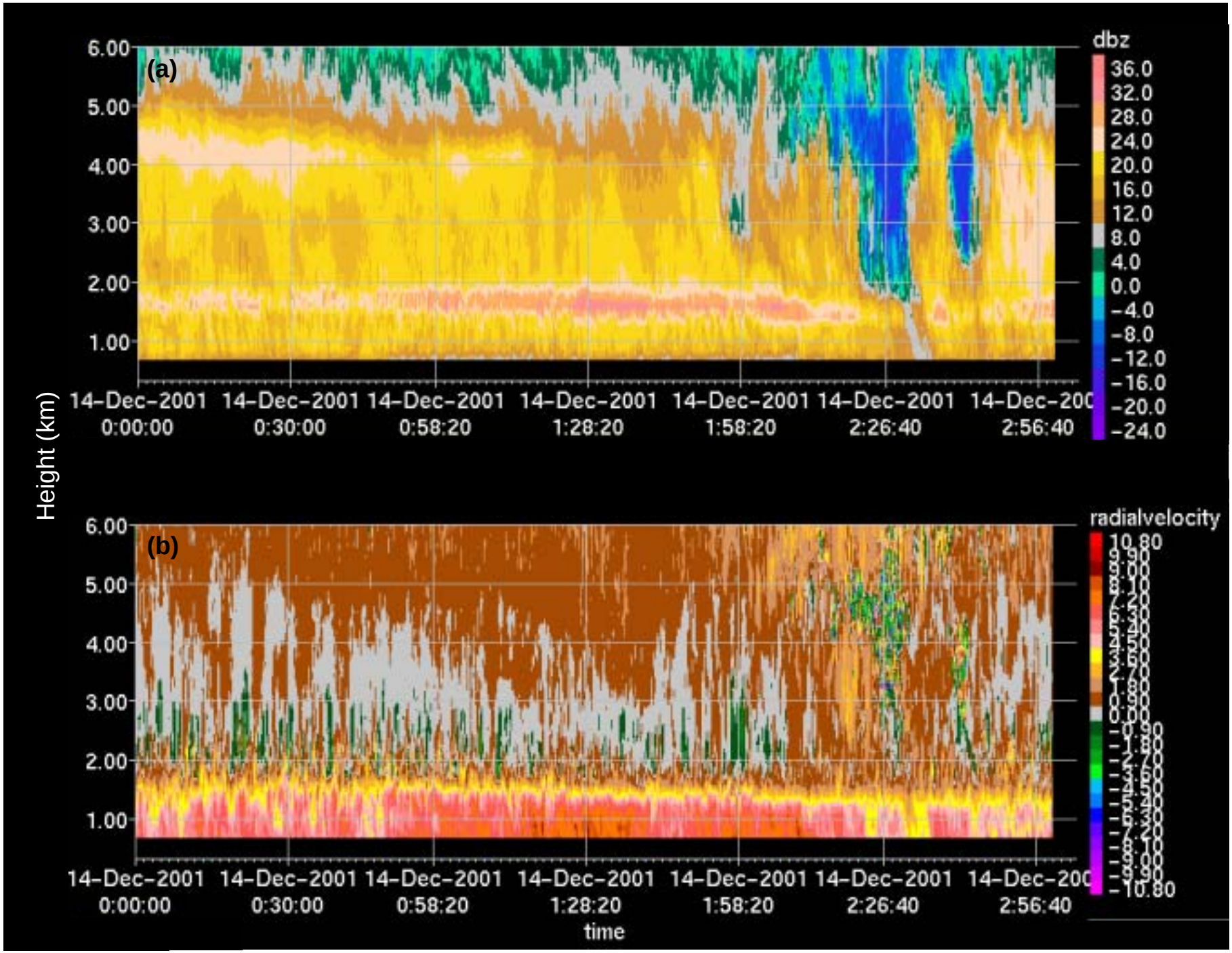

Stoelinga et al. Fig. 17. Time-height cross sections of measurements from the S-band profiler (see Fig. 3 for location) on 14 Dec 2001. (a) Reflectivity. (b) Doppler vertical velocity. Height is above sea-level, times are in UTC, and positive velocity values are downward.

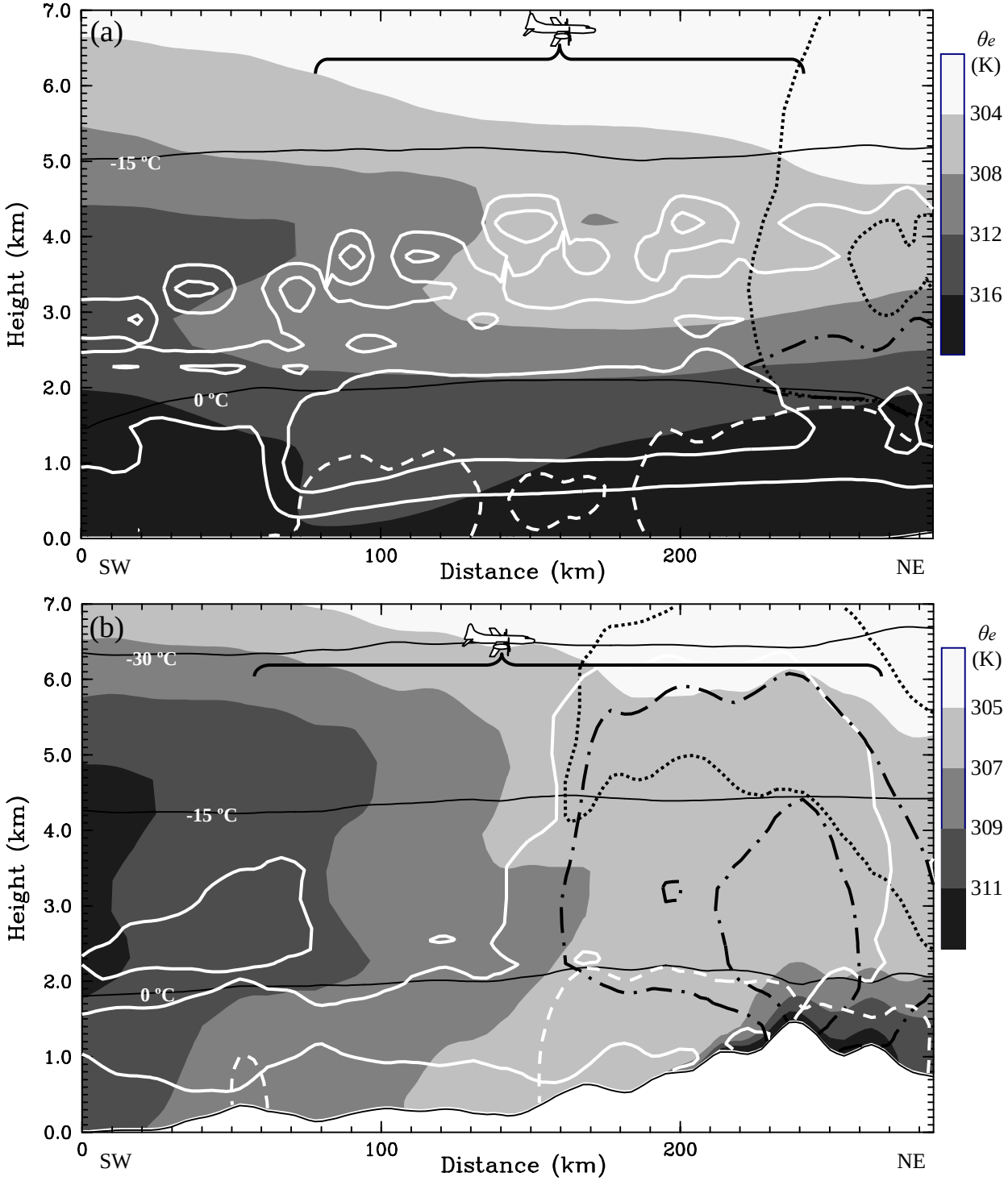

Stoelinga et al. Fig. 18. Cross sections through precipitation events simulated by the MM5 model on (a) 1-2 February 2001, and (b) 13-14 December 2001. Shading indicates equivalent potential temperature (θe), with key given at right. Thin black lines are temperature in ºC. Hydrometeor mixing ratios are indicated by contour types as follows: cloud water, solid white; rain, dashed white; snow, short-dashed black; and graupel, dash-dot black. Contour values in (a) are 0.1 g kg^{-1} for all types, and a second contour of 0.3 g kg^{-1} for cloud water and snow. Contour values in (b) are 0.2 g kg^{-1} for all types, and a second contour of 1.0 g kg^{-1} for cloud water and graupel. Regions covered by the UW Convair-580 flights are indicated by an aircraft symbol and large bracket.

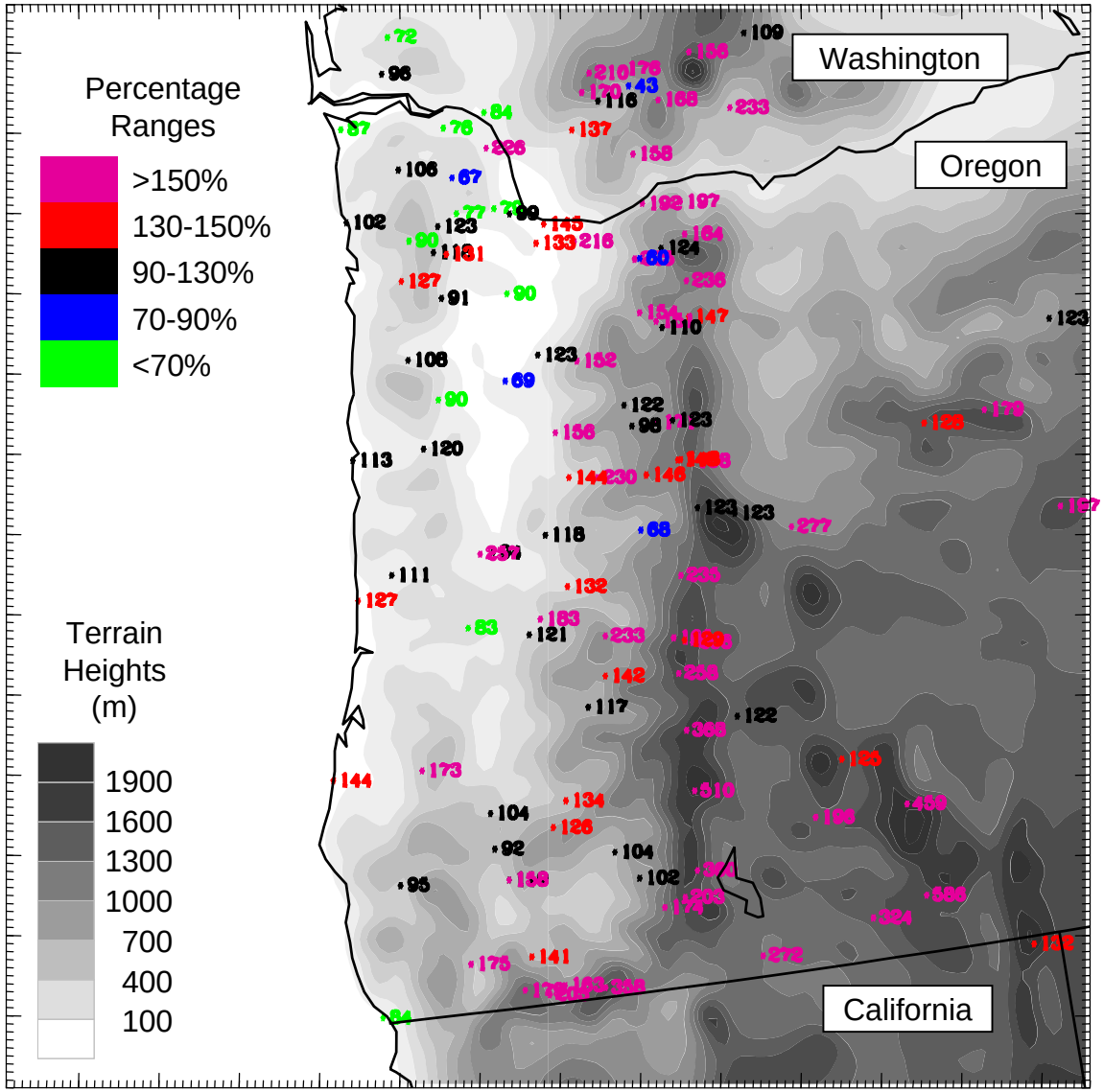

Stoelinga et al. Fig. 19. Precipitation accumulated during the period 1400 UTC 13 December 2002—0800 UTC 14 December 2002 from a 4-km MM5 model simulation, expressed as a percentage of observed precipitation at raingauge sites in the vicinity of the IMPROVE-2 study area. Terrain heights shown at lower left, and color coding of percentage ranges shown at upper left.